condensed with NLS-mu exhibited approximately 3 times higher NT scores than that of PLL, suggesting that NLS-mu enhances nuclear transfer. Carlisle *et al.* previously demonstrated the impact of hexon, a component of adenovirus, as a device for the nuclear delivery of polyethyleneimine (PEI)/pDNA particles by means of NT scores (denoted as frequency ratio in that paper) [22]. Since the doses of pDNA injected into the cytoplasm and nucleus were different, the absolute values of the NT scores cannot be directly compared between NLS-mu and hexon-modified PEI. However, based on results reported by Pollard *et al.* [7], the NT scores of pDNA condensed with PLL and PEI appear to be comparable. In addition, the NT score for PEI/pDNA particles increased by approximately 3-fold as the result of modification by hexon. Similarly, NLS-mu and mu also exhibited 2- and 3-fold higher NT scores compared with that of PLL. Taking these findings into consideration, the potential of NLS-mu to deliver pDNA is likely comparable to that of hexon.

Unexpectedly, the NT score for NLS-mu particles was comparable to that for mu, suggesting that the mu sequence, but not NLS_{SV40}, is responsible for the nuclear transfer process. Very recently, Keller *et al.* reported that the mu peptide also functions as a NLS since the fusion protein, which consists of mu and β-galactosidase, can efficiently accumulate in the nucleus [24]. Therefore, the mu sequence may be displayed on the particle and would also be recognized by nuclear-transport-associating proteins (i.e. importin). Concerning nuclear transfer, the influence of cell division should be also considered, since it is well accepted that nuclear delivery is efficiently achieved at cell division, when the nuclear membrane is temporarily disrupted [4,5,25,26]. As far as the number of RhoDex-positive cells is concerned, it is increased to the same degree during 24 h after cytoplasmic microinjection, regardless of the injected complexes. This observation indicates that the proportion of cell division is equivalent when various types of complexes are injected. With G1-arrested cells synchronized by hydroxyurea, it was revealed that the cells progress and undergo mitotic division within 15 h (data not shown). Since we measured transgene expression at 24 h post-injection, all of the cells should have divided at least once. It was previously reported that PLL was unlikely to function as a NLS [27]. Thus, the nuclear transfer of PLL/pDNA, corresponding to an NT score of 0.21, may be dominantly achieved at the cell division. In the case of mu and NLS-mu, the NT scores were determined to be 0.57 and 0.44, respectively. In this sense, contribution of nuclear transfer when achieved at the non-dividing phase was 63 and 52%, respectively.

As shown in Figure 1, all of the polycations had a particle size of approximately 80 nm at a charge ratio of 2. At a higher charge ratio, the sizes were correlated with the E(cyt) and NT scores. When the size was increased depending on the charge ratio in the NLS-mu particles, the E(cyt) values gradually decreased. The mechanism for the increased size is unknown. As summarized in Table 2, the NT score at a charge ratio of 10 was also decreased by approximately 50% compared with that at a charge ratio of 2. In contrast, the E(cyt) values of mu and PLL particles were not affected even at higher charge ratios, which is consistent with the unaltered particle size. These results suggest that the polycation/pDNA complex passed through the nuclear pore complex (NPC). However, this hypothesis is not consistent with a previous observation showing that a size threshold (~39 nm) exists for the passage of macromolecules through the NPC, as estimated using gold particles [28]. This may be explained by the difference in the flexibility of shape between gold particles and polycation/pDNA-condensed particles. The flexible shape of the polycation/pDNA-condensed particles could allow them to pass through the size limitation of the NPC (~39 nm). Alternatively, as proposed previously for PEI/pDNA complexes [22,29], they may overcome the nuclear pore-independent pathway. The underlying mechanism for the nuclear transfer of a polycation/pDNA complex currently remains to be elucidated. An inhibition study of nuclear delivery by the co-injection of wheat germ agglutinin (WGA) may aid in our understanding of the mechanism [22,30].

Concerning intra-nuclear transcription, the E(nuc) values were varied in the rank order of NLS-mu = PLL > mu. This suggests that the intra-nuclear transcription of pDNA, when condensed with mu, was inhibited. Considering that the E(nuc) value in pDNA condensed by NLS-mu at a higher charge ratio of 10 was significantly decreased compared with that condensed at a charge ratio of 2 (Table 2), tight condensation by a polycation appears to disturb transcription. Therefore, optimization of the release from the polycation is important for achieving an effective transcription process. It is noteworthy that the fusion of the NLS_{SV40} to the mu increased the E(nuc) value. Although the mechanism for this remains unclear, two explanations are possible. One is that the fusion of NLS_{SV40} induces recognition by the chaperone proteins, which are responsible for the nuclear remodeling of DNA. Examples of this include nucleoplasmin [31,32], nucleophosmin [33] and template activating factor-1 (TAF-1) [34,35]. The other is that the partial replacement of the arginine-rich residue derived from the mu to the lysine-rich residue derived from NLS_{SV40} physicochemically enhances the intra-nuclear release of pDNA. Plank *et al.* demonstrated that pDNA, when condensed with a lysine-rich polypeptide, is more easily released, compared to that condensed with an arginine-rich one [36].

Correctively, these data strongly suggest that the condensation of pDNA with a nuclear-targeting polycation is an excellent strategy for nuclear delivery. However, based on this strategy, it is necessary to optimize not only the efficiency of the nuclear delivery, but the subsequent intra-nuclear transcription, as well. In the present study, each process was separately evaluated by introducing a parameter, the NT score. As an ideal DNA condenser, we succeeded in developing a novel polycation, which has chimeric functions: an enhanced nuclear delivery

by mu and complementation of the impaired intranuclear transcription by NLS_{SV40}. This chimeric NLS-mu represents a potentially useful nuclear-targeting device for a non-viral gene vector.

Acknowledgements

This work was supported in part by Grants-in-Aid for Scientific Research (B) and Grant-in-Aid for Young Scientists (B) from the Ministry of Education, Culture, Sports, Science and Technology of Japan, and by Grants-in-Aid for Scientific Research on Priority Areas from the Japan Society for the Promotion of Science.

References

1. Akita H, Ito R, Khalil IA, *et al.* Quantitative three-dimensional analysis of the intracellular trafficking of plasmid DNA transfected by a nonviral gene delivery system using confocal laser scanning microscopy. *Mol Ther* 2004; **9**: 443–451.
2. Kamiya H, Akita H, Harashima H. Pharmacokinetic and pharmacodynamic considerations in gene therapy. *Drug Discov Today* 2003; **8**: 990–996.
3. Marenzi S, Adams RL, Zardo G, *et al.* Efficiency of expression of transfected genes depends on the cell cycle. *Mol Biol Rep* 1999; **26**: 261–267.
4. Mortimer I, Tam P, MacLachlan I, *et al.* Cationic lipid-mediated transfection of cells in culture requires mitotic activity. *Gene Ther* 1999; **6**: 403–411.
5. Tseng WC, Haselton FR, Giorgio TD. Mitosis enhances transgene expression of plasmid delivered by cationic liposomes. *Biochim Biophys Acta* 1999; **1445**: 53–64.
6. Wilke M, Fortunati E, van den Broek M, *et al.* Efficacy of a peptide-based gene delivery system depends on mitotic activity. *Gene Ther* 1996; **3**: 1133–1142.
7. Pollard H, Remy JS, Loussouarn G, *et al.* Polyethyleneimine but not cationic lipids promotes transgene delivery to the nucleus in mammalian cells. *J Biol Chem* 1998; **273**: 7507–7511.
8. Nagasaki T, Myohoji T, Tachibana T, *et al.* Can nuclear localization signals enhance nuclear localization of plasmid DNA? *Bioconjugate Chem* 2003; **14**: 282–286.
9. Tanimoto M, Kamiya H, Minakawa N, *et al.* No enhancement of nuclear entry by direct conjugation of a nuclear localization signal peptide to linearized DNA. *Bioconjugate Chem* 2003; **14**: 1197–1202.
10. Keller M, Tagawa T, Preuss M, *et al.* Biophysical characterization of the DNA binding and condensing properties of adenoviral core peptide mu. *Biochemistry* 2002; **41**: 652–659.
11. Kogure K, Moriguchi R, Sasaki K, *et al.* Development of a non-viral multifunctional envelope-type nano device by a novel lipid film hydration method. *J Control Release* 2004; **98**: 317–323.
12. Lechardeur D, Sohn KJ, Haardt M, *et al.* Metabolic instability of plasmid DNA in the cytosol: a potential barrier to gene transfer. *Gene Ther* 1999; **6**: 482–497.
13. Douglas JT. Adenovirus-mediated gene delivery to skeletal muscle. *Methods Mol Biol* 2004; **246**: 29–35.
14. Horellou P, Bilang-Bleuel A, Mallet J. In vivo adenovirus-mediated gene transfer for Parkinson's disease. *Neurobiol Dis* 1997; **4**: 280–287.
15. Timares L, Douglas JT, Tillman BW, *et al.* Adenovirus-mediated gene delivery to dendritic cells. *Methods Mol Biol* 2004; **246**: 139–154.
16. Subramanian A, Ranganathan P, Diamond SL. Nuclear targeting peptide scaffolds for lipofection of nondividing mammalian cells. *Nat Biotechnol* 1999; **17**: 873–877.
17. Rudolph C, Plank C, Lausier J, *et al.* Oligomers of the arginine-rich motif of the HIV-1 TAT protein are capable of transferring plasmid DNA into cells. *J Biol Chem* 2003; **278**: 11 411–11 418.
18. Li S, Huang L. In vivo gene transfer via intravenous administration of cationic lipid-protamine-DNA (LPD) complexes. *Gene Ther* 1997; **4**: 891–900.
19. Li S, Rizzo MA, Bhattacharya S, *et al.* Characterization of cationic lipid-protamine-DNA (LPD) complexes for intravenous gene delivery. *Gene Ther* 1998; **5**: 930–937.
20. Rittner K, Benavente A, Bompard-Sorlet A, *et al.* New basic membrane-destabilizing peptides for plasmid-based gene delivery in vitro and in vivo. *Mol Ther* 2002; **5**: 104–114.
21. Kakudo T, Chaki S, Futaki S, *et al.* Transferrin-modified liposomes equipped with a pH-sensitive fusogenic peptide: an artificial viral-like delivery system. *Biochemistry* 2004; **43**: 5618–5628.
22. Carlisle RC, Bettinger T, Ogris M, *et al.* Adenovirus hexon protein enhances nuclear delivery and increases transgene expression of polyethylenimine/plasmid DNA vectors. *Mol Ther* 2001; **4**: 473–483.
23. Masuda T, Akita H, Harashima H. Evaluation of nuclear transfer and transcription of plasmid DNA condensed with protamine by microinjection: The use of a nuclear transfer score. *FEBS Lett* 2005; **579**: 2143–2148.
24. Keller M, Harbottle RP, Perouzel E, *et al.* Nuclear localisation sequence templated nonviral gene delivery vectors: investigation of intracellular trafficking events of LMD and LD vector systems. *Chembiochemistry* 2003; **4**: 286–298.
25. Brunner S, Furtbauer E, Sauer T, *et al.* Overcoming the nuclear barrier: cell cycle independent nonviral gene transfer with linear polyethyleneimine or electroporation. *Mol Ther* 2002; **5**: 80–86.
26. Brunner S, Sauer T, Carotta S, *et al.* Cell cycle dependence of gene transfer by lipoplex, polyplex and recombinant adenovirus. *Gene Ther* 2000; **7**: 401–407.
27. Chan CK, Jans DA. Enhancement of polylysine-mediated transferrinfection by nuclear localization sequences: polylysine does not function as a nuclear localization sequence. *Hum Gene Ther* 1999; **10**: 1695–1702.
28. Pante N, Kann M. Nuclear pore complex is able to transport macromolecules with diameters of about 39 nm. *Mol Biol Cell* 2002; **13**: 425–434.
29. Godbey WT, Wu KK, Mikos AG. Tracking the intracellular path of poly(ethylenimine)/DNA complexes for gene delivery. *Proc Natl Acad Sci U S A* 1999; **96**: 5177–5181.
30. Yoneda Y, Imamoto-Sonobe N, Yamaizumi M, *et al.* Reversible inhibition of protein import into the nucleus by wheat germ agglutinin injected into cultured cells. *Exp Cell Res* 1987; **173**: 586–595.
31. McLay DW, Clarke HJ. Remodelling the paternal chromatin at fertilization in mammals. *Reproduction* 2003; **125**: 625–633.
32. Prieto C, Saperas N, Arnan C, *et al.* Nucleoplasmin interaction with protamines. Involvement of the polyglutamic tract. *Biochemistry* 2002; **41**: 7802–7810.
33. Okuwaki M, Iwamatsu A, Tsujimoto M, *et al.* Identification of nucleophosmin/B23, an acidic nucleolar protein, as a stimulatory factor for in vitro replication of adenovirus DNA complexed with viral basic core proteins. *J Mol Biol* 2001; **311**: 41–55.
34. Haruki H, Gyurcsik B, Okuwaki M, *et al.* Ternary complex formation between DNA-adenovirus core protein VII and TAF-Ibeta/SET, an acidic molecular chaperone. *FEBS Lett* 2003; **555**: 521–527.
35. Matsumoto K, Okuwaki M, Kawase H, *et al.* Stimulation of DNA transcription by the replication factor from the adenovirus genome in a chromatin-like structure. *J Biol Chem* 1995; **270**: 9645–9650.
36. Plank C, Tang MX, Wolfe AR, *et al.* Branched cationic peptides for gene delivery: role of type and number of cationic residues in formation and in vitro activity of DNA polyplexes. *Hum Gene Ther* 1999; **10**: 319–332.

articles

molecular pharmaceutics

Distribution of Immunoglobulin Fab Fragment Conjugated with HIV-1 REV Peptide following Intravenous Administration in Rats

Shouju Kameyama,*,† Ritsuko Okada,† Takeo Kikuchi,† Takao Omura,† Ikuhiko Nakase,‡ Toshihide Takeuchi,‡ Yukio Sugiura,‡ and Shiroh Futaki‡

Research Planning, Bipha Corporation, Chitose, Hokkaido 066-0051, Japan, and Institute for Chemical Research, Kyoto University, Uji, Kyoto 611-0011, Japan

Received August 22, 2005

Abstract: HIV-1 REV peptide (positions 34−50) is well-known as a cell-permeating peptide. In this study, we investigated the distribution of Fab fragment of immunoglobulin conjugated with REV peptide (REV-Fab) following intravenous administration in rats, and compared with those of the native Fab fragment (nFab). Radioiodinated REV-Fab or nFab (^{125}I-REV-Fab or ^{125}I-nFab, respectively) was given in a single intravenous dose of 2 mg/kg (3 MBq/kg). Total radioactive and TCA-insoluble radioactive concentrations in blood, whole-body autoradiography (ARG), and urinary excretion rates were assayed following administration. Regarding blood and plasma, total radioactive and TCA-insoluble radioactive concentrations for ^{125}I-REV-Fab were remarkably lower than those for ^{125}I-nFab. In the whole-body ARG at 4 h after administration, ^{125}I-REV-Fab produced remarkably higher radioactivity in the adrenal gland, spleen, and liver, compared to ^{125}I-nFab. Regarding urinary excretion rates, approximately 70% of the radioactive dose was excreted in the form of a low-molecular-weight component by 24 h after administration for both samples. ^{125}I-REV-Fab may penetrate quickly from blood to adrenal gland, spleen, liver, and other tissues after intravenous administration to rats, and then did not stay in situ and was digested and excreted mostly via the renal route by 24 h. With these features, cell-permeating peptides are expected to help the development of new antibody pharmaceuticals.

Keywords: Whole-body autoradiography; HIV-1 derived REV peptide (positions 34−50); immunoglobulin Fab fragment; intravenous administration; cell-permeating peptide

Introduction

Immunoglobulin preparations contain many kinds of antibodies against viruses, bacteria, and the like and are widely used for the prevention and treatment of infectious diseases. Although these antibodies are effective in blood vessels and humoral fluids, they are unable to be fully effective, due to their inability to permeate the cell membrane of infected cells, against viruses, bacteria, and the like that have gone into latency in cells or tissues after infection. In recent years, many studies have been reported on the new finding that a series of arginine-rich peptides allow polymeric substances to penetrate into cells.[1−5] Against this background,

* Corresponding author: Shouju Kameyama, General manager, Research planning, Bipha Corporation, 1007-124, Izumisawa, Chitose, Hokkaido, 066-0051, Japan. Phone: +81-072-856-9389. Fax: +81-072-864-2341. E-mail: Kameyama.Shouju@mm.m-pharma.co.jp.

† Bipha Corporation.

‡ Kyoto University.

(1) Fawell, S.; Seery, J.; Daikh, Y.; Moore, C.; Chen, L. L.; Pepinsky, B.; Barsoum, J. Tat-mediated delivery of heterologous proteins into cells. *Proc. Natl. Acad. Sci. U.S.A.* **1994**, *91*, 664−668.

(2) Vives, E.; Brodin, P.; Lebleu, B. A truncated HIV-1 tat protein basic domain rapidly translocates through the plasma membrane and accumulates in the cell nucleus. *J. Biol. Chem.* **1997**, *272*, 16010−16017.

(3) Derossi, D.; Joliot, A. H.; Chassaing, G.; Prochiantz, A. The third helix of the Antennapedia homeodomain translocates through biological membranes. *J. Biol. Chem.* **1994**, *269*, 10444−10450.

10.1021/mp050064m CCC: $33.50
Published on Web 12/08/2005

we are studying such cell-permeating peptides with the aim of their application to the development of new drugs having the potential for penetration into cells and tissues conferred by binding immunoglobulin and the peptides.

Of the various cell-permeating peptides, the peptide derived from the TAT protein, an HIV-1 transcription factor, has been studied extensively and reported to show very quick penetration into cells and tissues. Studies of the pharmacokinetics and tissue distribution of this peptide are ongoing, and research programs aiming at the clinical application of drugs incorporating the peptide are being implemented.[6−10] Meantime, taking note of the identity of the TAT peptide as an arginine-rich sequence, we have shown that some new peptides are also capable of penetrating into cells.[11−15] The HIV-1-derived REV protein, in particular, like the TAT protein, is known to play a key role in nuclear export of the mRNAs,[16] and we showed that the peptide corresponding to positions 34−50, the site for binding to nucleic acid (RRE),[17] is highly capable of penetrating into cells.[11] In this study, we attempted to add a new function of intracellular penetration to immunoglobulin by binding it to the REV peptide.

There are only a very few studies of complexes of the REV peptide and high-molecular-weight proteins, with almost no reports available on complexes of the REV peptide and immunoglobulin or its functional fragment. Furthermore, although some studies are available on the penetration into cells in vitro, there are almost no reports on the distribution or tissue penetration. So, we conjugated the REV peptide to the Fab fragment of immunoglobulin and gave the resulting complex to rats by a single intravenous administration to examine its disposition. The complex of the REV peptide and the Fab fragment was prepared using a convenient method based on chemical modification,[11] rather than a gene recombination procedure. The Fab fragment was prepared from a polyclonal antibody preparation containing many different kinds of antibodies,[18] and was labeled with ^{125}I by the chloramine-T method.[19,20] Its distribution was analyzed by whole-body autoradiography, a method known to serve as an excellent tool for the accurate analysis of the kinetics of labeled drugs in animal bodies, and changes in its concentrations in blood and plasma over time and its urinary excretion were also determined.

Methods and Materials

Preparation of Immunoglobulin Fab Fragment. The immunoglobulin Fab fragment (nFab) used was prepared from a commercially available human polyclonal antibody preparation (Venoglobulin-IH, Mitsubishi Pharma, Japan) using the ImmunoPure Fab Preparation Kit (Pierce Chemical Company, USA).

Conjugation of REV Peptide to nFab. The REV peptide (TRQAR RNRRR RWRER QRGC) was chemically synthesized by the Peptide Institute Inc. (Osaka, Japan). Its purity was 95.1% as determined by HPLC. Conjugation of nFab with REV peptide was similarly carried out as reported previously.[11] An *N*-(6-maleimidocaproyloxy) succinimide

(4) Derossi, D.; Chassaing, G.; Prochiantz, A. Trojan peptides: the penetratin system for intracellular delivery. *Trends Cell Biol.* **1998**, *8*, 84−87.
(5) Nagahara, H.; Vocero-Akbani, A. M.; Snyder, E. L.; Ho, A.; Latham, D. G.; Lissy, N. A.; Becker-Hapak, M.; Ezhevsky, S. A.; Dowdy, S. F. Transduction of full-length TAT fusion proteins into mammalian cells: TAT-p27^{Kip1} induces cell migration. *Nat. Med.* **1998**, *4*, 1449−1452.
(6) Schwarze, S. R.; Ho, A.; Vocero-Akbani, A.; Dowdy, S. F. In vivo transduction: delivery of a biological active protein into mouse. *Science* **1999**, *285*, 1569−1572.
(7) Lee, H. J.; Pardridge, W. M. Pharmacokinetics and delivery of tat and tat-protein conjugates to tissues in vivo. *Bioconjugate Chem.* **2001**, *12*, 995−999.
(8) Bullok, K. E.; Dyszlewski, M.; Prior, J. L.; Pica, C. M.; Sharma, V.; Piwnica-Worms, D. Characterization of novel Histidine-tagged tat-peptide complexes dual-labeled with ^{99m}Tc-tricarbonyl and fluorescein for scintigraphy and fluorescence microscopy. *Bioconjugate Chem.* **2002**, *13*, 1226−1237.
(9) Silhol, M.; Tyagi, M.; Giacca, M.; Lebleu, B.; Vives, E. Different mechanisms for cellular internalization of the HIV-1 tat-derived cell penetrating peptide and recombinant proteins fused to tat. *Eur. J. Biochem.* **2002**, *269*, 494−501.
(10) Wadia, J. S.; Dowdy, S. F. Protein transduction technology. *Curr. Opin. Biotechnol.* **2002**, *12*, 52−56.
(11) Futaki, S.; Suzuki, T.; Ohashi, W.; Yagami, T.; Tanaka, S.; Ueda, K.; Sugiura, Y. Arginine-rich peptides: an abundant source of membrane-permeable peptides having potential as carriers for intracellular protein delivery. *J. Biol. Chem.* **2001**, *276*, 5836−5840.
(12) Futaki, S.; Nakase, I.; Suzuki, T.; Zhang, Y.; Sugiura, Y. Translocation of branched-chain arginine peptides through cell membranes: flexibility in the spatial disposition of positive charges in membrane-permeable peptides. *Biochemistry* **2002**, *41*, 7925−7930.
(13) Futaki, S. Arginine-rich peptides: potential for intracellular delivery of macromolecules and the mystery of the translocation mechanisms. *Int. J. Pharm.* **2002**, *245*, 1−7.
(14) Futaki, S.; Goto, S.; Sugiura, Y. Membrane permeably commonly shared among arginine-rich peptides. *J. Mol. Recognit.* **2003**, *16*, 260−264.
(15) Nakase, I.; Miwa, M.; Takeuchi, T.; Sonomura, K.; Kawabata, N.; Koike, Y.; Takehashi, M.; Tanaka, S.; Ueda, K.; Simpson, J. C.; Jones, A. T.; Sugiura, Y.; Futaki, S. Cellular uptake of arginine-rich peptides: Roles for macropinocytosis and actin rearrangement. *Mol. Ther.* **2004**, *10*, 1011−1022.
(16) Malim, M. H.; Hauber, J.; Fenrick, R.; Cullen, B. R. Immunodeficiency virus rev trans-activator modulates the expression of the viral regulatory genes. *Nature* **1988**, *335*, 181−183.
(17) Kumagai, I.; Takahashi, T.; Hamasaki, K.; Ueno, A.; Mihara, H. Construction of HIV rev peptides containing peptide nucleic acid that bind HIV RRE IIB RNA. *Bioorg. Med. Chem. Lett.* **2000**, *10*, 377−379.
(18) Mage, M. G. Preparation of Fab fragments from IgGs of different animal species. *Methods Enzymol.* **1980**, *70*, 142−150.
(19) Sonoda, S.; Schlamowitz, M. Studies of 125I trace labeling of immunoglobulin G by chloramine-T. *Immunochemistry* **1970**, *7*, 885−898.
(20) Stavrou, D.; Mellert, W.; Bilzer, T.; Senekowitsch, R.; Keiditsch, E.; Mehraein, P. Radioimmunodetection of gliomas by administration of radiolabelled monoclonal antibodies. Experimental data. *Anticancer Res.* **1985**, *5*, 147−156.

ester (EMCS) solution, equivalent to 120 μg of EMCS, was added to 1 mL of 1 mg/mL nFab solution, and this mixed solution was gently stirred at room temperature for 2 h. The reaction liquor was treated with a PD-10 column (Amersham), equilibrated previously, to remove excess EMCS. Subsequently, the column effluent was concentrated by centrifugation using Microprep (Millipore, USA), and phosphate-buffered saline (PBS) was added to make a final volume of 1 mL. A REV peptide solution, equivalent to 600 μg of the peptide, was added to this solution, and the mixture was gently stirred at room temperature for 2 h. The excess portion of the REV peptide was removed using a PD-10 column, the column effluent was concentrated by centrifugation using Microprep (Millipore), PBS was added to make a final concentration of 1 mg/mL, and this solution was stored under refrigeration until use.

Iodine Labeling of REV-Fab or nFab. The REV-Fab or nFab fraction was labeled with ^{125}I by the chloramine-T method.[19,20] Twenty micrograms of protein was incubated with 37 MBq (1 mCi) of [^{125}I]Na (Amersham, France) and chloramine T (10 nmol) in Eppendorf tubes for 30−60 s at room temperature. The reaction was quenched by the addition of sodium meta-bisulfite (62 nmol). Free iodine was removed by chromatography on a PD-10 Sephadex G-25 column (Amersham, Les Ulis, France). Iodine labeling of REV-Fab or nFab was prepared by the addition of nonlabeled REV-Fab or nFab to 2 mg/mL. Specific activity ranged about 1.5 MBq/mg for REV-Fab or nFab.

Uptake into HeLa cells. HeLa cells were seeded on 24-well plate at a density of 2.5−5.0 × 10^4 cells per well. After a subconfluent state was reached, the culture medium was replaced with 500 μL of MEM medium, and the plate was allowed to stand in an incubator at 37 °C for 3 h. Subsequently, 5 μL of the test substance was added and reacted under the specified conditions, after which the plate was washed three times by PBS, a trypsin-EDTA solution was added, and the reaction was carried out at 37 °C for at least 15 min to completely detach the cells. The cells and cell lysate were recovered from each well to a polystyrene tube, and radioactivity was determined using a gamma counter (COBRA Quantum; PerkinElmer, Meriden, CT).

Intravenous Administration of REV-Fab or nFab. Male Sprague-Dawley rats were given free access to food and water. Each rat was weighed (288−307 g) and housed in a metabolic cage for collection of urine and feces at 24 h. Rats received a single bolus dose of 2 mg/kg (3 MBq/kg, 80 μCi/kg) of ^{125}I-REV-Fab or ^{125}I-nFab via the femoral vein. This dosage was selected to be identical with that employed for the clinically used antibody drugs.[21]

Determination of Blood and Plasma Concentrations. At 0.25, 0.5, 1, 3, 6, and 24 h after administration of the test substance, blood (approximately 0.4 mL) was drawn from the caudal vein using a glass capillary having its inner wall treated with 500 units/mL heparin sodium in physiological saline. A 0.1 mL portion of each blood sample was separated for determination of blood concentrations, and the remaining portion was quickly centrifuged (3000 rpm, 15 min, 4 °C) to separate plasma. These blood samples were stored under ice-cooling conditions until plasma separation. Prior to every time of blood drawing, the animals were examined for macroscopic signs. A 0.1 mL portion of blood or plasma was transferred to a polystyrene tube, and the radioactivity in the sample was determined using a gamma counter. Subsequently, 1 mL of physiological saline and 1 mL of 20% TCA were added to the assayed sample, and this was followed by centrifugation (3000 rpm, 15 min, 4 °C). The supernatant was removed, 1 mL of physiological saline was added to the sediment, followed by centrifugation in the same manner, the supernatant was removed, and the radioactivity in the TCA sediment fraction was determined.

Whole-Body ARG. Animals receiving the test substance were killed by ether anesthesia at 4 h after administration. After each animal was clipped, an approximately 3% carboxymethylcellulose sodium salt (CMC-Na) solution was used to fill in the oral cavity, nasal cavities, ear holes, and anus, and the animal was quickly frozen in a hexane−Dry Ice bath. The tail and extremities were then amputated, and the body was preserved in wrap at −20.4 to −17.0 °C for at least 24 h. An approximately 3% aqueous solution of CMC-Na was applied to the body surface of the frozen fixed rat. Subsequently, the body was embedded in an approximately 5% aqueous solution of CMC-Na and frozen in a hexane−Dry Ice bath to obtain a frozen block. Frozen sections 30 μm in thickness were prepared using a cryomicrotome. The sections obtained involved a median plane, a renal plane, and 2 planes of major tissues. Each section was freeze-dried at approximately −20 °C. The dry section was applied to base paper and covered with Mylar film. This section for ARG was brought into close contact with an imaging plate (IP) and exposed to radiation in a shield box for 12 h. After completion of the exposure, readings were taken using a bioimaging analyzer, and a whole-body ARGM was generated (gradation, 65 536; resolution, 50 μm; sensitivity, 4000; latitude, 5; IP, BAS-MS2040). Images obtained by whole-body ARG were analyzed on a relative basis using the Image Gauge software program (version 3.46, Fuji Photo Film, Japan).

Determination of Urinary Excretion. Animals receiving the test material were placed in metabolic cages, and all urine was pooled for a period of 0−24 h after administration (1 plot in total). These urine samples were collected under ice-cooling conditions. After urine sampling, the inside of the metabolic cage was washed with an appropriate amount of 50% methanol, and the washings were recovered. The volumes of urine and cage washings were quantified, and, as required, purified water was added for the purpose of

(21) Cobleigh, M. A.; Vogel, C. L.; Tripathy, D.; Robert, N. J.; Scholl, S.; Fehrenbacher, L.; Wolter, J. M.; Paton V.; Shak, S.; Lieberman, G.; Slamon, D. J. Multinational study of the effecacy and safty of humanized anti-HER2 monoclonal antibody in women who have HER2-overexpressing metastatic breast cancer that has progressed after chemotherapy for metastatic disease. *J. Clin. Oncol.* **1999**, *17*, 2639−2648.

dilution. A 0.2 mL portion of this urine sample and washings was transferred to a polystyrene tube, and the radioactivity in the sample was determined using a gamma counter. Subsequently, 1 mL of physiological saline and 1 mL of 20% TCA were added to the assayed sample, and this was followed by centrifugation (3000 rpm, 15 min, 4 °C). The supernatant was removed, 1 mL of physiological saline was added to the sediment, followed by centrifugation in the same manner, the supernatant was removed, and the radioactivity in the TCA sediment fraction was determined.

Excretion rates were determined as the percent ratio of radioactivity in urine and washings to the dosed radioactivity. After background was subtracted from the measured values of radioactivity in urine and washings, the ratio to the dosed radioactivity (actual measured value) was calculated. The excretion rates of the radioactivity in the washings and the radioactivity in urine were separately calculated, and the two values were summed to obtain the overall urinary excretion rate.

Results

Penetration of Test Samples into HeLa Cells. ^{125}I-nFab or ^{125}I-REV-Fab was added to the culture medium for subconfluent HeLa cells, and their uptake into the cells was examined. Figure 1A shows the dose dependent curves for ^{125}I-nFab and ^{125}I-REV-Fab to incorporate in the cells. The cell-associated protein level of ^{125}I-REV-Fab was increased with dose dependence from 1.25 nM to 400 nM, but that of ^{125}I-nFab was very low to 400 nM. As shown in Figure 1B for time-related changes in uptake, ^{125}I-REV-Fab was incorporated in the cells in a very short time, but the incorporation level of ^{125}I-nFab was very low for 60 min. In this experiment, the cells were treated with trypsin prior to the radioactivity measurements. This trypsin treatment effectively removes the surface-adsorbed proteins,[16] and therefore, the majority of the radioactivity can be attributed to the internalized Fabs. The internalization of fluorescently labeled REV-Fab was also confirmed by confocal microscopic observation (data not shown). The effectiveness of the REV segment as a delivery vector was thus verified.

Radioactive Concentrations in Blood and Plasma. Figures 2 and 3 shows total radioactive concentrations in blood and plasma and radioactive concentrations in the TCA-insoluble fraction following intravenous administration of ^{125}I-nFab or ^{125}I-REV-Fab.

Following administration of ^{125}I-nFab, the total radioactive concentration in blood was 9149 ± 324 ng equiv/mL at 0.25 h after administration, the first measuring time point, after which the concentration decreased in a biphasic pattern and became 274 ± 29 ng equiv/mL at 24 h after administration. The radioactive concentration in plasma was 16 839 ± 1643 ng equiv/mL of ^{125}I-nFab at 0.25 h, after which the concentration decreased in a biphasic pattern and became 377 ± 37 ng equiv/mL at 24 h. The ratio of TCA-insoluble radioactive concentration to total radioactivity for ^{125}I-nFab was approximately 92.0% and 93.2% in blood and plasma at 0.25 h, respectively, after which it decreased until 6 h and became approximately 36.5% and 22.6%, respectively, and then, it recovered to 69.3% and 60.3% at 24 h, respectively (Table 1).

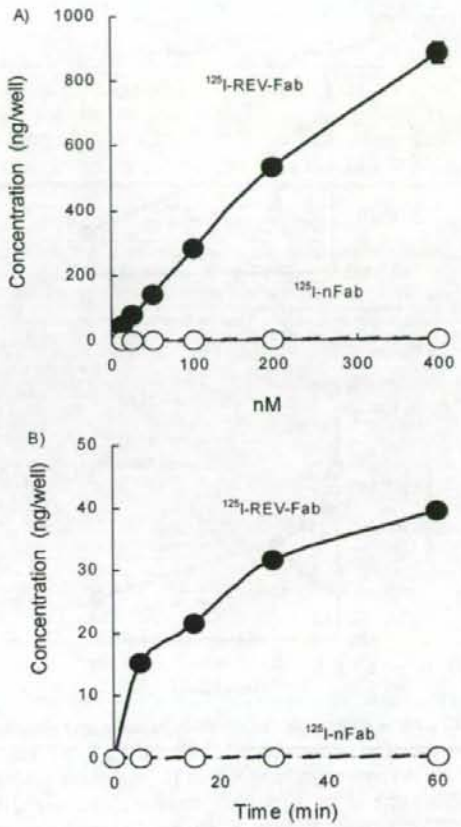

Figure 1. Uptake of ^{125}I-REV-Fab or ^{125}I-nFab into HeLa cells. (A) Concentration−response curve for ^{125}I-REV-Fab (●) or ^{125}I-nFab (○). HeLa cells were incubated for 30 min in the medium containing test sample with concentrations from 1.25 to 400 nM (corresponding to 0.04 and 12 μg of protein/well, respectively). (B) Time course of response to ^{125}I-REV-Fab (●) or ^{125}I-nFab (○). HeLa cells were treated with antibodies at a concentration of 20 nM (0.6 μg of protein/well). At different time points the cells were washed and trypsinized. The cell-associated ^{125}I-proteins (ordinate) were estimated from radioacitivity of trypsinized cell and cell lysate, reported per well of a 24-well plate, and presented as mean ± SD of four wells.

Following administration of ^{125}I-REV-Fab, the total radioactive concentration in blood was 2619 ± 767 ng equiv/mL at 0.25 h, a level approximately $^{1}/_{3.5}$ of the concentration observed with ^{125}I-nFab, after which the concentration decreased in a biphasic pattern and became 356 ± 92 ng equiv/mL at 24 h after administration. The total radioactive concentration in plasma decreased to 3949 ± 772 ng equiv/mL, a level approximately $^{1}/_{4.3}$ of those with ^{125}I-nFab, and this was followed by a biphasic reduction. The ratio of TCA-insoluble radioactive concentration to total radioactivity for ^{125}I-REV-Fab in blood was approximately 83.9% and 80.7%

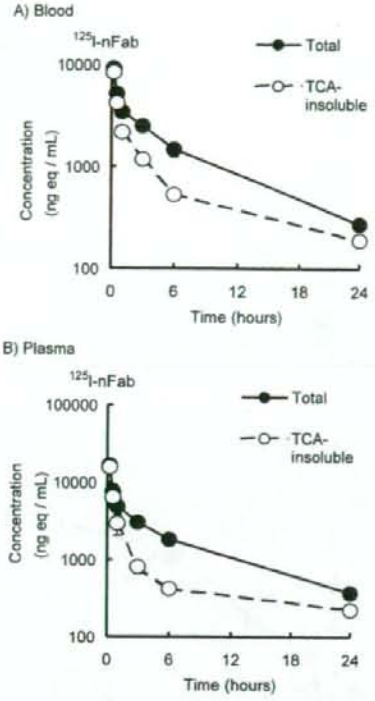

Figure 2. Concentrations of radioactivity in blood and plasma after intravenous administration of ^{125}I-nFab to male rats. Total radioactivity (●) and the radioactivity of TCA-insoluble pellets (○) were measured by a gamma counter. Data are the mean ± SD of the results from 3 animals. Concentration of radioactivity is shown as the corresponding amount of ^{125}I-labeled proteins yielding equivalent radioactivity (ng equiv/mL).

in blood and plasma, respectively, at 0.25 h, after which it decreased until 6 h and became approximately 42.9% and 13.9%, respectively, and then it recovered to 65.6% and 55.4% respectively (Table 2).

Whole-Body Autoradiography. Radioactivity distributions at 4 h after intravenous administration of ^{125}I-nFab or ^{125}I-REV-Fab are shown in Figures 4 and 5, respectively. First, for ^{125}I-nFab, particularly high radioactivity was observed in the thyroid, renal cortex, intracystic urea, and gastric contents, and relatively high radioactive concentrations were observed in the skin, whereas almost no radioactivity was detected in the brain, spinal cord, or eyeballs. For ^{125}I-REV-Fab, high radioactive concentrations were detected in the thyroid, renal cortex, gastric contents, intracystic urea, and skin, whereas almost no radioactivity was detected in the brain, spinal cord, or eyeballs, as with ^{125}I-nFab. However, for ^{125}I-REV-Fab, high radioactive concentrations were also observed in the spleen, liver, and adrenal gland.

Urinary Excretion. Table 3 shows the urinary radioactive excretion rates following intravenous administration of ^{125}I-nFab or ^{125}I-REV-Fab. The urinary excretion rates for ^{125}I-nFab and ^{125}I-REV-Fab were 71.2 ± 14.8% and 69.5 ± 4.5%, respectively, by 24 h after administration. The ratio of TCA sedimentable fraction to total urinary radioactivity was 0.38% and 0.04%, respectively. Therefore, the majority of radioactivity would be derived from low-molecular-weight components containing free or peptide-bound ^{125}I, because the TCA-insoluble radioactivity corresponds to the intact

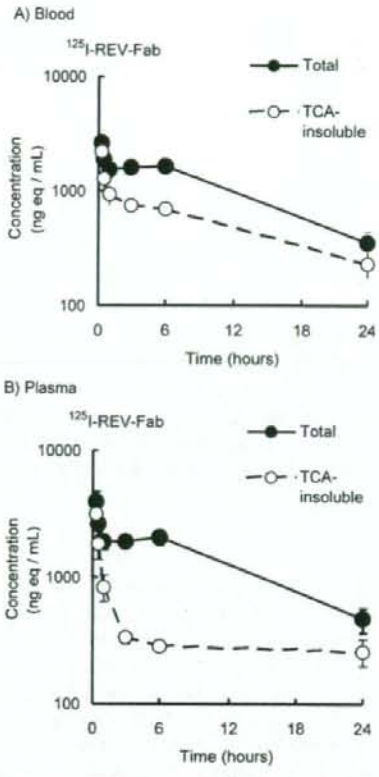

Figure 3. Concentrations of radioactivity in blood and plasma after intravenous administration of ^{125}I-REV-Fab to rats. Total radioactivity (●) and the radioactivity of TCA-insoluble pellets (○) were measured by a gamma counter. Data are the mean ± SD of the results from 3 animals. Concentration of radioactivity is shown as the corresponding amount of ^{125}I-labeled proteins yielding equivalent radioactivity (ng equiv/mL).

Table 1. TCA-Insoluble Radioactivity Ratio after Intravenous Administration of ^{125}I-nFab to Male Rats

time after administration[a] (h)	TCA-insoluble radioactivity ratio (%)[b]	
	in blood	in plasma
0.25	92.0 ± 4.8	93.2 ± 0.7
0.5	81.8 ± 7.6	83.7 ± 2.4
1.0	63.8 ± 1.6	58.9 ± 4.4
3.0	46.9 ± 1.4	26.5 ± 3.4
6.0	36.5 ± 4.6	22.6 ± 0.7
24.0	69.3 ± 4.2	60.3 ± 6.0

[a] Time after intravenous administration of ^{125}I-nFab. [b] The ratio of TCA-insoluble radioactivity per total radioactivity in blood or plasma. Data are the mean ± SD of the results from 3 animals.

Table 2. TCA-Insoluble Radioactivity Ratio after Intravenous Administration of ^{125}I-REV-Fab to Male Rats

time after administration[a] (h)	TCA-insoluble radioactivity ratio (%)[b]	
	in blood	in plasma
0.25	83.9 ± 1.7	80.7 ± 1.7
0.5	63.3 ± 1.3	69.2 ± 4.9
1.0	60.6 ± 3.2	44.0 ± 5.2
3.0	46.6 ± 1.6	17.6 ± 0.5
6.0	42.6 ± 1.1	13.9 ± 1.3
24.0	65.6 ± 0.9	55.4 ± 5.3

[a] Time after intravenous administration of ^{125}I-REV-Fab. [b] The ratio of TCA-insoluble radioactivity per total radioactivity in blood or plasma. Data are the mean ± SD of the results from 3 animals.

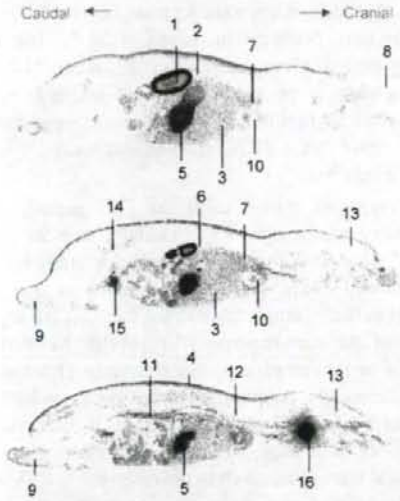

Figure 4. Whole-body autoradiograms at 4 h after intravenous administration of ^{125}I-nFab to male rat. Each number indicates responsible organs. 1: Kidney. 2: Spleen. 3: Liver. 4: Skin. 5: Gastric contents. 6: Adrenal gland. 7: Lung. 8: Eyeball. 9: Testis. 10: Heart. 11: Blood. 12: Spinal cord. 13: Brain. 14: Bone marrow. 15: Urinary bladder. 16: Thyroid gland.

REV-Fab as well as partially digested proteins having relatively high molecular weights.

Discussion

A recent study has revealed that high-molecular-weight substances can be incorporated in cells through the cell membrane when bound with certain basic peptides, though they are otherwise unable to penetrate into cells.[22-24] On the TAT peptide, in particular, many reports are available, including a great deal of research into its kinetics in animal

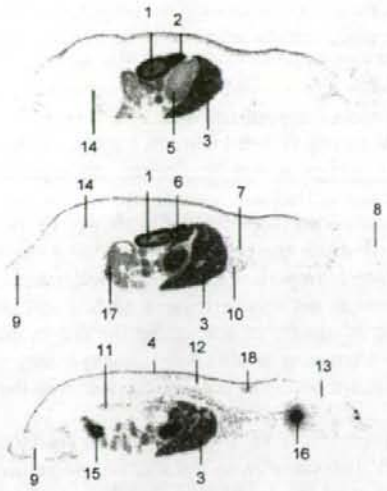

Figure 5. Whole-body autoradiograms at 4 h after intravenous administration of ^{125}I-REV-Fab to male rat. Each number indicates responsible organs. 1: Kidney. 2: Spleen. 3: Liver. 4: Skin. 5: Gastric contents. 6: Adrenal gland. 7: Lung. 8: Eyeball. 9: Testis. 10: Heart. 11: Blood. 12: Spinal cord. 13: Brain. 14: Bone marrow. 15: Urinary bladder. 16: Thyroid gland. 17: Intestinal contents. 18: Brown fat.

Table 3. Urinary Excretion of Radioactivity in 24 h after Intravenous Administration of ^{125}I-REV-Fab or ^{125}I-nFab to Male Rats

samples	urinary excretion	
	% of dose[a]	% of TCA-insoluble[b]
^{125}I-REV-Fab	69.5 ± 4.5	0.04 ± 0.00
^{125}I-nFAB	71.2 ± 14.8	0.38 ± 0.15

[a] Total urinary excretion of radioactivity per total radioactivity of dose. [b] The ratio of TCA-insoluble radioactivity per total urinary radioactivity. Data are the mean ± SD of the results from 3 animals.

bodies and in blood, as well as intracellular uptake,[25-27] and studies are ongoing to apply it to the treatment of various diseases.[28-31] Additionally, since the TAT peptide has an

(22) Eguchi, A.; Akuta, T.; Okuyama, H.; Senda, T.; Yokoi, H.; Inokuchi, H.; Fujita, S.; Hayakawa, T.; Takeda, K.; Hasegawa, M.; Nakanishi, M. Protein transduction domain of HIV-1 Tat protein promotes efficient delivery of DNA into mammalian cells. *J. Biol. Chem.* **2001**, *276*, 26204−26210.

(23) Nakanishi, M.; Eguchi, A.; Akuta, T.; Nagoshi, E.; Fujita, S.; Okabe, J.; Senda, T.; Hasegawa, M. Basic peptides as functional components of non-viral gene transfer vehicles. *Curr. Protein Pept. Sci.* **2003**, *4*, 141−150.

(24) Lewin, M.; Carlesso, N.; Tung, C. H.; Tang, X. W.; Cory, D.; Scadden, D. T.; Weissleder, R. Tat peptide-derived magnetic nanoparticles allow in vivo tracking and recovery of progenitor cells. *Nat. Biotechnol.* **2000**, *18*, 410−414.

(25) Wadia, J. S.; Dowdy, S. F. Modulation of cellular function by TAT mediated transduction of full length proteins. *Curr. Protein Pept. Sci.* **2003**, *4*, 97−104.

(26) Ziegler, A.; Nervi, P.; Dürrenberger, M.; Seeling, J. The cationic cell-penetrating peptide CPP^{TAT} derived from the HIV-1 protein TAT is rapidly transported into living fibroblasts: optical, biophysical, and metabolic evidence. *Biochemistry* **2005**, *44*, 138−148.

arginine-rich sequence, other arginine-rich peptides of protein origin have also been studied extensively; peptides from the HIV-1 REV protein or the FHV coat,[32] like the TAT peptide, have been shown to be capable of allowing high-molecular-weight substances to penetrate into cells.

The REV protein is well-known as a nuclear exporter of the mRNAs, and its activity is of paramount importance to the proliferation of the virus; accordingly, many reports have been presented on the suppression of its activity. On the other hand, we found that the peptide corresponding to position 34−50, which is important to the transcription activity of the REV protein, not only serves as a nucleic acid binding site but also is capable of permeating the cell membrane. We are now attempting to add a new function of intracellular penetration to antibodies by conjugating them with the REV peptide.

In the present study, we first examined the uptake of ^{125}I-labeled REV-Fab complex in HeLa cells, and verified the efficient and quick incorporation of the ^{125}I-labeled complex into the cells with the help of the REV peptide. Subsequently, the disposition and blood kinetics following intravenous administration in rats were investigated using this RI-labeled complex. The blood and plasma concentrations of ^{125}I-REV-Fab decreased very rapidly in the initial phase following intravenous administration; conversely, in the terminal phase, ^{125}I-REV-Fab decreased more slowly than ^{125}I-nFab. Regarding whole-body ARG, the time point for comparison was set to be 4 h after administration, when the initial rapid change had been complete and a transition to gradual decline occurred. We demonstrated that ^{125}I-REV-Fab produced remarkably greater accumulation of radioactivity in the adrenal gland, spleen, and liver compared with ^{125}I-nFab. The rapid initial decreases in blood and plasma concentrations following administration of ^{125}I-REV-Fab can be explained by the penetration of ^{125}I-REV-Fab to these organs, resulting in significantly lower concentrations than those of ^{125}I-nFab. The slow elimination from plasma in the terminal phase is also attributable to the gradual liberation of tissue-incorporated ^{125}I-REV-Fab complex from the tissue to blood. Since the TCA-insoluble fraction content was high at approximately 90% in the initial phase after administration but decreased to approximately 60% in the terminal phase, and also since the TCA sediment fraction content in urine decreased to less than 1%, it was postulated that ^{125}I-REV-Fab underwent decomposition to low-molecular-weight components in tissue and then excreted in urine. These results suggested that the incorporated labeled complex did not stay in situ for a long time, with approximately 70% of the dose excreted via the renal route in the form of low-molecular-weight components by 24 h after administration. TCA-insoluble radioactivity ratios were decreased over a 6 h period after iv injection, but then increased at 24 h. The total radioactivity decreased consistently between 6 and 24 h after iv injection, whereas the decrease in TCA-insoluble radioactivity was not so significant. This eventually yielded the apparent increase in the TCA-insoluble radioactivity ratios at 24 h after injection.

Several reports of studies using the TAT peptide show high pulmonary uptake, as well as accumulation in the spleen and liver,[6−8] whereas the results of the present study for ^{125}I-REV-Fab showed almost no uptake in pulmonary tissue. This difference is partially attributable to the fact that the reports on the use of the conventional TAT peptide handled the peptide as is or its complex with a substance of relatively low molecular weight. Additionally, it has been reported that a complex of TAT and β galactosidase was incorporated in the brain as of 8 h after administration when given by intraperitoneal administration.[6] In the case of ^{125}I-REV-Fab, however, almost no radioactivity was observed in the brain, spine, or eyeballs, though the determination was made at 4 h after administration. It remains unclear whether these differences are due to differences in the kind of protein modified, or to differences in the kind of cell-membrane-permeating peptide used.

The above results demonstrate that ^{125}I-REV-Fab penetrates into organs in a very short time following intravenous administration in vivo, as well as its intracellular penetration in vitro. Furthermore, its disposition was found to occur in accumulative pattern in particular organs, such as the spleen, liver, and adrenal gland, rather than in a uniform distribution to all organs. It was also shown that the incorporated labeled complex did not stay in situ for a long time, with approximately 70% of the dose excreted via the renal route in the form of low-molecular-weight components by 24 h after administration. With these features, cell-permeating peptides are expected to help the development of new antibody pharmaceuticals.

Acknowledgment. We are grateful to Dr. Takatoshi Nakamura (Shin Nippon Biomedical Lab., Japan) for helpful discussions.

MP050064M

(27) Brooks, H.; Lebleu, B.; Vives, E. Tat peptide-mediated cellular delivery: back to basics. *Adv. Drug Delivery Rev.* **2005**, *57*, 559−577.

(28) Schwarze, S. R.; Hruska, K. A.; Dowdy, S. F. Protein transduction: Unrestricted delivery into all cells? *Trends Cell Biol.* **2000**, *10*, 290−295.

(29) Polyakov, V.; Sharma, V.; Dahlheimer, J. L.; Pica, C. M.; Luker, G. D.; Piwnica-Worms, D. Novel tat-peptide chelates for direct transduction of technetium-99m and rhenium into human cells for imaging and radiotherapy. *Bioconjugate Chem.* **2000**, *11*, 762−771.

(30) Niesner, U.; Halin, C.; Lozzi, L.; Gunthert, M.; Neri, P.; Wunderli-Allenspach, H.; Zardi, L.; Neri, D. Quantitation of the tumor-targeting properties of antibody fragments conjugated to cell-permeating HIV-1 tat peptides. *Bioconjugate Chem.* **2002**, *13*, 729−736.

(31) Rothbard, J. B.; Garlington, S.; Lin, Q.; Kirschberg, T.; Kreider, E.; McGrane, P. L.; Wender, P. A.; Khavari, P. A. Conjugation of arginine oligomers to cyclosporin A facilitates topical delivery and inhibition of inflammation. *Nat. Med.* **2000**, *6*, 1253−1257.

(32) Futaki, S.; Goto, S.; Suzuki, T.; Nakase, I.; Sugiura, Y. Structural variety of membrane permeable peptides. *Curr. Protein Pept. Sci.* **2003**, *4*, 87−96.

Case Report

Pediatric Neurosurgery

Pediatr Neurosurg 2006;42:240–244
DOI: 10.1159/000092362

Received: April 13, 2005
Accepted: September 30, 2005

Successful Chemotherapy for Congenital Malignant Gliomas: A Report of Two Cases

Takashi Tamiya[a,b] Soichiro Takao[b] Tomotsugu Ichikawa[b]
Kosuke Chayama[c] Isao Date[b]

[a]Department of Neurological Surgery, Kagawa University School of Medicine, Kagawa, and Departments of [b]Neurological Surgery and [c]Pediatrics, Okayama University Graduate School of Medicine, Okayama, Japan

Key Words
Chemotherapy · Congenital glioma · Anaplastic astrocytoma · Malignant ganglioglioma

Abstract
We describe the cases of 2 patients with a congenital malignant glioma that responded to chemotherapy. In the first case, a 2-month-old boy had a conjugate deviation to the right side and nystagmus. A T_1-weighted gadolinium-enhanced magnetic resonance image showed a large tumor in his right frontal lobe. The tumor was partially resected, and the histological diagnosis was malignant ganglioglioma. The child then underwent 6 cycles of chemotherapy (mainly carboplatin and etoposide), and the residual tumor shrank. The tumor was then partially resected during a second operation, after which the patient underwent 5 cycles of chemotherapy (a combination of carboplatin, etoposide, vincristine, ifosfamide, cisplatin and cyclophosphamide). The tumor has not recurred in more than 8.5 years. In the second case, a 2-month-old boy had bulging of the anterior fontanel. The T_1-weighted gadolinium-enhanced magnetic resonance image showed a large suprasellar tumor. The tumor was partially resected, and the histological diagnosis was anaplastic astrocytoma. The patient underwent 8 cycles of chemotherapy (MCNU, carboplatin and etoposide) and the tumor has not recurred in more than 7.5 years. Our experience indicates that, if surgical removal and chemotherapy are done aggressively for malignant gliomas in neonates and infants, long-term survival is possible.

Introduction

Congenital brain tumors are uncommon [1] and a variety of definitions of 'congenital' have been proposed. Solitare and Krigman [2] specified three categories of congenital brain tumors: (1) definitely congenital – present or producing symptoms at birth; (2) probably congenital – present or producing symptoms within the first week; (3) possibly congenital – present or producing symptoms within the first months of life. The period of 2 months, first proposed by Arnstein et al. [3], is the more widely accepted limit for defining congenital brain tumors [1, 4], and several cases of congenital malignant gliomas, including glioblastomas, have been reported [5–12].

Herein, we describe 2 cases of congenital malignant gliomas in 2-month-old infants who have survived in the long term after subtotal removal and chemotherapy without irradiation.

KARGER
Fax +41 61 306 12 34
E-Mail karger@karger.ch
www.karger.com

1016–2291/06/0424–0240$23.50/0

Accessible online at:
www.karger.com/pne

Takashi Tamiya, MD
Department of Neurological Surgery
Kagawa University School of Medicine, 1750-1 Ikenobe
Miki-cho, Kida-gun, Kagawa 761-0793 (Japan)
Tel. +81 87 891 2207, Fax +81 87 891 2208, E-Mail tamiya@med.kagawa-u.ac.jp

Case Reports

Case 1

This infant boy was delivered at 40 weeks gestation after a normal pregnancy and had no neurological signs or symptoms at birth. At 2 months of age, he was unable to converge his eyes toward a common point or follow movement with his eyes. His eyes deviated to the right and he also had horizontal nystagmus. Computed tomography (CT) revealed a huge tumor in his right parietal lobe, and he was subsequently admitted to our hospital on July 29, 1996.

At the time of admission, the patient's head circumference was 42.5 (± 1.3 SD) cm and there was no bulge in his fontanel. Magnetic resonance imaging (MRI) showed a huge intra-axial lesion in the right frontal lobe, which was mostly hypo- and isointense on the T_1-weighted image and heterogeneously hyperintense on the T_2-weighted image with abnormal enhancement after the administration of gadolinium (fig. 1). The patient underwent partial resection of the tumor, which was white and soft and had a strong tendency to bleed. The border of the tumor was not clearly demarcated, and small sections adhering to the optic nerve and the carotid artery were left behind. On histopathological examination, the tumor was composed of two regions, one with high cellularity and the other with low cellularity. In the region with high cellularity, abundant mitotic figures were observed. At least several mitotic figures were found in the sites where mitosis was most prominent (fig. 2A). In the region with low cellularity, the cells were large and had a bright cytoplasm. Their nucleoli were observed clearly, and mitotic figures were not seen (fig. 2B). Some short fusiform cells were positive for glial fibrillary acidic protein (GFAP) staining (fig. 2C). According to these findings, the tumor was diagnosed as a malignant ganglioglioma.

The patient's postoperative course was uneventful and he began a chemotherapy regimen consisting mainly of carboplatin in a daily dose of 500 mg/m^2 for 3 days and etoposide in a daily dose of 150 mg/m^2 for 5 days. He underwent 6 cycles of this chemotherapy. The residual tumor shrank, and a second resection of the tumor was done through the craniotomy. The tumor was not removed completely, since part of it was adjacent to the right optic nerve and the right internal carotid artery. The histopathological findings for the specimen removed during the second operation showed that the tumor was similar to the region with low cellularity obtained from the specimen from the first operation. Mitotic figures were almost undetected (fig. 2D).

The patient's second postoperative course was uneventful and his neurological signs did not worsen. He began 5 cycles of chemotherapy consisting mainly of 500 mg/m^2 carboplatin for 3 days and 150 mg/m^2 etoposide for 5 days in combination with ifosfamide, vincristine, cisplatin and cyclophosphamide. During chemotherapy, he developed anemia due to bone marrow suppression, leukopenia and thrombopenia, which were corrected with a transfusion of concentrated erythrocyte and thrombocyte preparations and G-CSF. The tumor's size did not increase during or after chemotherapy. The patient had no other severe side effects of the chemotherapy and was discharged from the hospital. For the past 8.5 years, he has lived a normal daily life, although his mental development is slightly retarded. Follow-up MRIs show that the tumor has not enlarged (fig. 3).

Fig. 1. Case 1. The preoperative gadolinium-enhanced MRI showed a huge intra-axial enhanced mass in the right frontal lobe.

Case 2

This infant boy was delivered at 40 weeks gestation after a normal pregnancy and had no neurological signs or symptoms at birth. A local physician noticed his bulging fontanel at 2 months of age and found a suprasellar tumor on an MRI. The boy was admitted to our hospital on July 2, 1997.

At the time of admission, the patient was 62 cm in height and 6.3 kg in weight. His eyes deviated to the left and he had horizontal nystagmus. His fontanel was bulging. An MRI revealed a huge suprasellar lesion, with abnormal homogeneous enhancement after the administration of gadolinium (fig. 4). The patient underwent a partial resection of the tumor, the border of which was not well demarcated. A small piece of tumor was left surrounding the optic nerve.

Histopathological examination showed that relatively homogeneous, short, fusiform cells proliferated in the tumor. The tumor was dense with blood vessels, and vascular endothelial cells proliferated markedly. Mitotic figures were abundant (fig. 5A), and most of the cells were positive for GFAP staining (fig. 5B). According to these findings, the tumor was diagnosed as an anaplastic astrocytoma.

The patient had no neurological deficits after the operation and his postoperative course was uneventful. He underwent 8 cycles of chemotherapy consisting of 80 mg/m^2 MCNU for 1 day, 500 mg/m^2 carboplatin for 1 day and 80 mg/m^2 etoposide for 3 days. Thereafter, the tumor decreased. While undergoing chemotherapy, the patient developed anemia due to bone marrow suppression, which resolved after an infusion of concentrated erythrocyte preparations. He had no other severe side effects of the chemotherapy and was discharged from the hospital. For the past 7.5 years, he has lived a normal daily life, with mild mental retardation and mild hemiplegia on the left side. Follow-up MRIs show that the tumor has not enlarged (fig. 6).

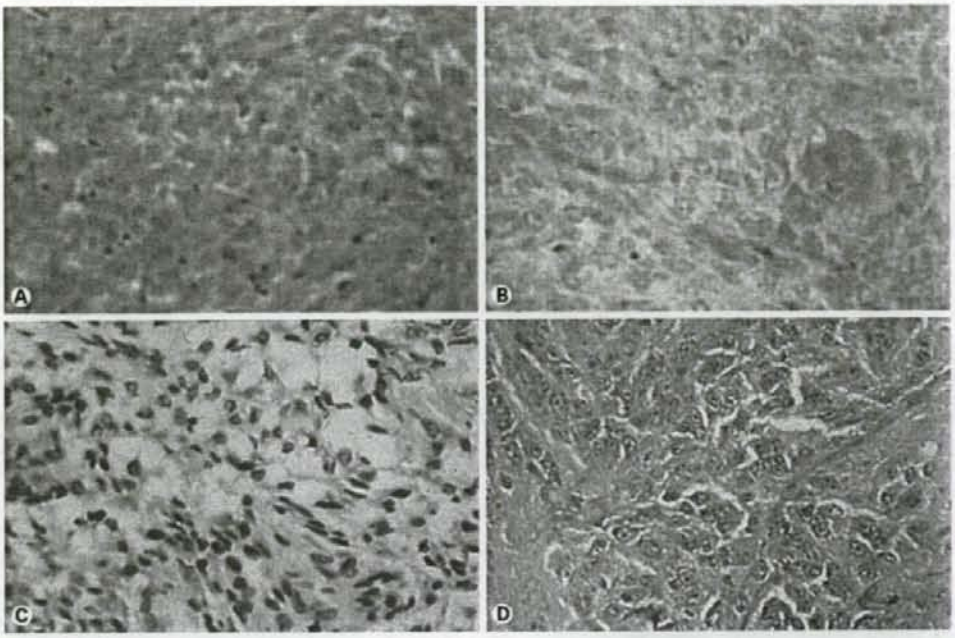

2

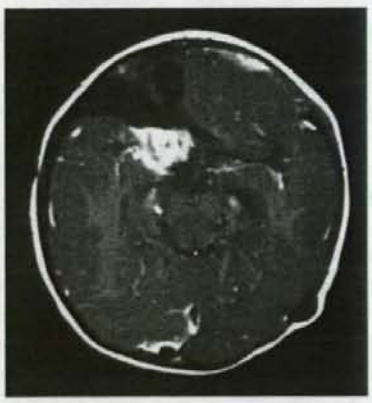

3

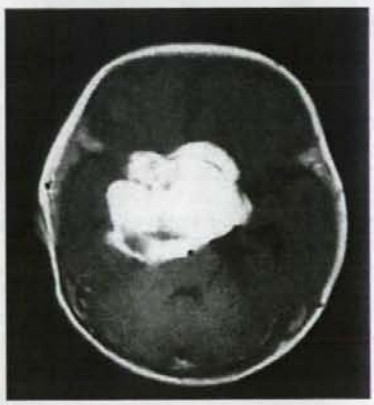

4

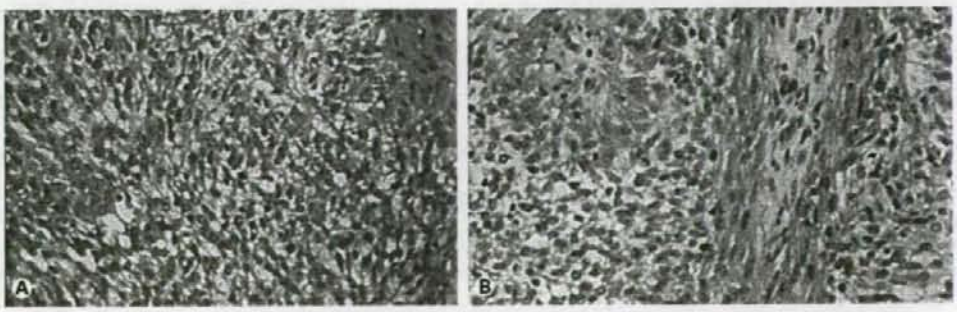

5

Discussion

According to several reports, brain tumors in children under the age of 1 year comprise 5.4% [1], 7.7% [4] or 13% [13] of all brain tumors in children. The probability of detecting brain tumors in patients under the age of 1 year seems to have increased concomitantly with the development of diagnostic instruments such as CT and MRI [1, 4, 13, 14]. The definition of a 'congenital tumor' is still obscure. Solitare and Krigman [2] divided congenital brain tumors into three categories: (1) definitely congenital – present or producing symptoms at birth; (2) probably congenital – present or producing symptoms within the first week; (3) possibly congenital – present or producing symptoms within the first few months of life. The period of 2 months, first proposed by Arnstein et al. [3], is more widely accepted as the limit for defining congenital brain tumors [1, 4]. According to Arnstein's definition, our 2 patients had cases of congenital tumor. Both patients had symptoms at 2 months, and the MRIs showed already huge tumors in their brains.

6

Fig. 2. Case 1. Histopathological photomicrographs depicting the results of hematoxylin and eosin staining (**A**, **B**) and GFAP staining (**C**) of the tumor from the first operation, and hematoxylin and eosin staining (**D**) of the tumor from the second operation. Original magnification ×100. The tumor from the first operation was composed of two regions, one with high cellularity and the other with low cellularity. **A** In the region with high cellularity, abundant mitotic figures were seen. **B** In the region with low cellularity, cells were large and had a bright cytoplasm. Their nucleoli were observed clearly. **C** GFAP staining showed that some short fusiform cells were positive. **D** The tumor from the second operation was similar to the region with low cellularity in the specimen obtained from the first operation. Mitotic figures were almost undetected.

Fig. 3. Case 1. The gadolinium-enhanced MRI showed that part of the tumor remained but was not enlarged 8.5 years after the first operation.

Fig. 4. Case 2. The preoperative gadolinium-enhanced MRI revealed a huge suprasellar lesion with abnormal homogeneous enhancement.

Fig. 5. Case 2. Histopathological photomicrographs depicting the results of hematoxylin and eosin staining (**A**) and GFAP staining (**B**) of the tumor. **A** Relatively homogeneous, short fusiform cells proliferated in the tumor. The density of blood vessels was high, and vascular endothelial cells proliferated markedly. Abundant mitotic figures were seen. **B** Most of the cells were positive for GFAP staining.

Fig. 6. Case 2. The gadolinium-enhanced MRI showed that a small part of the tumor remained but was not enlarged 7.5 years after the operation.

Malignant gliomas in children are rare, but they are almost as aggressive as in adults, resisting therapy, progressing rapidly and – not uncommonly – disseminating [15]. Malignant gliomas in children under the age of 1 year resist multidisciplinary therapy and often have a poor prognosis [14]. In addition, brain tumors in infants are often detected after they have grown to a huge size. Consequently, the prognosis for an infant with a brain tumor has generally been considered poor [1, 4, 13, 16, 17]. The most effective treatment for gliomas in infants is not only to remove them as safely and extensively as possible [18], but also to supplement the surgical resection with subsequent chemotherapy or radiation therapy. It is generally agreed, however, that radiation should be avoided in infants and children under the age of 3 years to prevent potential mental, intellectual and endocrine disorders [19]. Thus, chemotherapy has an important role in treating congenital malignant gliomas.

Several kinds of multi-drug chemotherapy, consisting of different combinations of various agents, have been given to infants with malignant glioma [15, 16, 20–22]. In the only randomized trial to investigate the effectiveness of chemotherapy in treating high-grade astrocytomas in children, Sposto et al. [20], found that chemotherapy consisting of chloroethyl cyclohexyl nitrosourea, vincristine and prednisone prolonged survival and event-free survival. Duffner et al. [21] also reported that chemotherapy with cyclophosphamide, vincristine, cisplatin and etoposide appears to be an effective primary postoperative treatment for many malignant brain tumors in young children. Recently, Massimino et al. [15] found that sequential, high-dose chemotherapy using cisplatin, etoposide, vincristine, cyclophosphamide, high-dose methotrexate and thiotepa, with harvesting of peripheral blood progenitor cells, could be used as front-line therapy for childhood malignant gliomas without excessive morbidity. On the other hand, Finlay et al. [23], reported that there was no benefit to treating high-grade astrocytomas

in children with 8-drugs-in-1-day chemotherapy compared with CCNU, vincristine and prednisone, and that the overall outcome for children with high-grade astrocytomas remained poor. Heideman et al. [16] also found that neoadjuvant chemotherapy was not associated with a survival rate significantly different from that observed in adjuvant chemotherapy studies. Our study used multidrug chemotherapy mainly consisting of carboplatin and etoposide in combination with ifosfamide, vincristine, cisplatin and cyclophosphamide in the first patient, and chemotherapy consisting of MCNU, carboplatin and etoposide in the second. Both patients had favorable results for the long term. We found that, even when a part of the tumor had to be left behind to preserve function, multidrug chemotherapy effectively reduced the size of congenital malignant gliomas. Therefore, we believe that multi-drug chemotherapy should be administered aggressively.

Several cases of congenital malignant gliomas, including glioblastomas, have been reported [5–12], and some patients survived in the long term after surgical resection and chemotherapy [6, 9, 12]. Hall et al. [24] described a case of anaplastic ganglioglioma in an infant who did well for 20 months after the operation without evidence of tumor recurrence on subsequent CT scans. Winters et al. [9] suggested that the biological behavior of congenital glioblastoma multiforme might not be as unfavorable as portrayed in the literature or as seen in adults. Therefore, we believe that aggressive treatment to remove the tumor as safely and extensively as possible, supplemented by subsequent chemotherapy, should be carried out for infants with malignant gliomas.

References

1 Furuta T, Tabuchi A, Adachi Y, Mizumatsu S, Tamesa N, Ichikawa T, Tamiya T, Matsumoto K, Ohmoto T: Primary brain tumors in children under age 3 years. Brain Tumor Pathol 1998;15:7–12.

2 Solitare GB, Krigman MR: Congenital intracranial neoplasm: a case report and review of the literature. J Neuropathol Exp Neurol 1964; 23:280–292.

3 Arnstein LH, Boldrey E, Naffziger HC: A case report and survey of brain tumors during the neonatal period. J Neurosurg 1951;8:315–319.

4 Jooma R, Hayward RD, Grant DN: Intracranial neoplasms during the first year of life: Analysis of one hundred consecutive cases. Neurosurgery 1984;14:31–41.

5 Mazzone D, Magro G, Lucenti A, Grasso S: Report of a case of congenital glioblastoma multiforme: an immunohistochemical study. Childs Nerv Syst 1995;11:311–313.

6 Pizer BL, Moss T, Oakhill A, Webb D, Coakham HB: Congenital astroblastoma: an immunohistochemical study. Case report. J Neurosurg 1995;83:550–555.

7 Narita T, Kurotaki H, Hashimoto T, Ogawa Y: Congenital oligodendroglioma: a case report of a 34th-gestational week fetus with immunohistochemical study and review of the literature. Hum Pathol 1997;28:1213–1217.

8 Price DB, Miller LJ, Drexler S, Schneider SJ: Congenital ganglioglioma: report of a case with an unusual imaging appearance. Pediatr Radiol 1997;27:748–749.

9 Winters JL, Wilson D, Davis DG: Congenital glioblastoma multiforme: a report of three cases and a review of the literature. J Neurol Sci 2001;188:13–19.

10 Morof DF, Levine D, Stringer KF, Grable I, Folkerth R: Congenital glioblastoma multiforme: prenatal diagnosis on the basis of sonography and magnetic resonance imaging. J Ultrasound Med 2001;20:1369–1375.

11 Nakayama K, Nakamura Y: Related localization of congenital glioblastomas in the Japanese: a case report and review of the literature. Childs Nerv Syst 2002;18:149–152.

12 Shimamura N, Asano K, Ogane K, Yagihashi A, Ohkuma H, Suzuki S: A case of definitely congenital glioblastoma manifested by intratumoral hemorrhage. Childs Nerv Syst 2003;19: 778–781.

13 Rocco CD, Ceddia A, Iannelli A: Intracranial tumours in the first year of life: a report on 51 cases. Acta Neurochir (Wien) 1993;123:14–24.

14 Haddad SF, Menezes AH, Bell WE, Godersky JC, Afifi KA, Bale JF: Brain tumors occurring before 1 year of age: a retrospective review of 22 cases in an 11-year period. Neurosurgery 1991;29:8–13.

15 Massimino M, Gandola L, Luksch R, Spreafico F, Riva D, Solero C, Giangaspero F, Locatelli F, Podda M, Bozzi F, Pignoli E, Collini P, Cefalo G, Zecca M, Casanova M, Ferrari A, Terenziani M, Meazza C, Polastri D, Scaramuzza D, Ravagnani F, Fossati-Bellani F: Sequential chemotherapy, high-dose thiotepa, circulating progenitor cell rescue, and radiotherapy for childhood high-grade glioma. Neuro-Oncology 2005;7:41–48.

16 Heideman RL, Kuttesch J Jr, Gajjar AJ, Walter AW, Jenkins JJ, Li Y, Sanford RA, Kun LE: Supratentorial malignant gliomas in childhood: a single institution perspective. Cancer 1997;80:497–504.

17 Graham ML, Herndon JE 2nd, Casey JR, Chaffee S, Ciocci GH, Krischer JP, Kurtzberg J, Laughlin MJ, Longee DC, Olson JF, Paleologus N, Pennington CN, Friedman HS: High-dose chemotherapy with autologous stem-cell rescue in patients with recurrent and high-risk pediatric brain tumors. J Clin Oncol 1997;15: 1814–1823.

18 Wisoff JH, Boyett JM, Berger MS, Brant C, Li H, Yates AJ, McGuire-Cullen P, Turski PA, Sutton LN, Allen JC, Packer RJ, Finlay JL: Current neurosurgical management and the impact of the extent of resection in the treatment of malignant gliomas of childhood: a report of the Children's Cancer Group trial No CCG-945. J Neurosurg 1998;89:52–59.

19 Danoff BF, Cowchock FS, Marquette C, Mulgrew L, Kramer S: Assessment of the long-term effects of primary radiation therapy for brain tumors in children. Cancer 1982;49: 1580–1586.

20 Sposto R, Ertel IJ, Jenkin RD, Boesel CP, Venes JL, Ortega JA, Evans AE, Wara W, Hammond D: The effectiveness of chemotherapy for treatment of high grade astrocytoma in children: results of a randomized trial. A report from the Childrens Cancer Study Group. J Neurooncol 1989;7:165–177.

21 Duffner PK, Horowitz ME, Krischer JP, Friedman HS, Burger PC, Cohen ME, Sanford RA, Mulhern RK, James HE, Freeman CR, Seidel FG, Kun LE: Postoperative chemotherapy and delayed radiation in children less than three years of age with malignant brain tumors. N Engl J Med 1993;328:1725–1731.

22 Rickert CH, Probst-Cousin S, Gullotta F: Primary intracranial neoplasms of infancy and early childhood. Childs Nerv Syst 1997;13: 507–513.

23 Finlay JL, Boyett JM, Yates AJ, Wisoff JH, Milstein JM, Geyer JR, Bertolone SJ, McGuire P, Cherlow JM, Tefft M, et al: Randomized phase III trial in childhood high-grade astrocytoma comparing vincristine, lomustine, and prednisone with the eight-drugs-in-1-day regimen. Childrens Cancer Group. J Clin Oncol 1995;13:112–123.

24 Hall WA, Yunis EJ, Albright AL: Anaplastic ganglioglioma in an infant: case report and review of the literature. Neurosurgery 1986;19: 1016–1020.

Novel Protein Transduction Method by Using 11R

An Effective New Drug Delivery System for the Treatment of Cerebrovascular Diseases

Tomoyuki Ogawa, MD; Shigeki Ono, MD, PhD; Tomotsugu Ichikawa, MD, PhD; Seiji Arimitsu, MD; Keisuke Onoda, MD, PhD; Koji Tokunaga, MD, PhD; Kenji Sugiu, MD, PhD; Kazuhito Tomizawa, MD, PhD; Hideki Matsui, MD, PhD; Isao Date, MD, PhD

Background and Purpose—A motif of 11 consecutive arginines (11R) is reported to be one of the most effective protein transduction domains for introducing proteins into the cell membrane. We therefore examined the transduction efficiency of 11R in cerebral arteries.

Methods—Basilar arteries (BAs) obtained from rats were incubated with either 11R-enhanced green fluorescent protein (11R-EGFP) or EGFP without 11R. After incubation, expression of 11R-EGFP or EGFP in BA serial sections was observed by fluorescence microscope. In an additional in vivo experiment, 11R-EGFP or EGFP was injected into the cisterna magna with or without subarachnoid hemorrhage. The 11R-EGFP or EGFP was injected just after the autologous blood injection, and then the expression of 11R-EGFP or EGFP in BA sections was also observed by fluorescence microscope.

Results—The 11R-EGFP signal was much stronger than that of EGFP in all layers of the rat BA, in both in vivo and ex vivo experiments. Moreover, the 11R-EGFP was transduced into the BA immediately (2 hours after the injection). Interestingly, 11R-fused fluorescent protein was transduced especially into the tunica media of the BA.

Conclusions—The 11R-fused fluorescent protein effectively penetrates into all layers of the rat BA, especially into the tunica media. This is the first study to our knowledge to demonstrate the successful transduction of a protein transduction domain fused protein into the cerebral arteries. **(*Stroke*. 2007;38:1354-1361.)**

Key Words: cerebral vasospasm ■ cerebrovascular disease protein ■ enhanced green fluorescence protein ■ transduction domain

Gene transfer by viral vectors is an attractive approach for studies of basic mechanisms of vascular biology, as well as for therapies for various vascular diseases, including cerebral vasospasm after subarachnoid hemorrhage (SAH), because viral vectors have the natural ability to enter cells and direct the expression of transgenes by infected host cells.[1–3] Actually, to date, there have been several experimental studies of gene transfer by adenovirus vector into cerebral vessels.[4–6]

Regarding the cerebral vessels, however, previous preclinical studies have shown that the efficiency of the adenoviral vector-mediated gene transfer is not sufficient for clinical use, because genes can be transferred only into the adventitia overlying cerebral vessels by transcisternal application.[4,7–9] Moreover, previous studies indicated that virus-mediated gene therapy has significant safety problems, such as inflammatory response, viral toxicity, and random integration of the viral vector's DNA into the host chromosomes.[10–12] Recent studies have shown that liposomes are able to deliver exogenous genes with minimal toxicity in vivo.[13–15] The efficiency of gene transduction is, however, worse than that of virus-mediated gene transfer at present.[10]

Previous studies have shown that a wide variety of proteins can be directly and harmlessly transduced into several different kinds of cells by conjugating short (10 to 16 residues long) peptides known as protein transduction domains (PTD). PTDs have been identified as critical domains necessary for effective protein transduction.[16–18] This new protein transduction method is believed to have some advantages over viral vector-mediated gene transduction in terms of safety, cell toxicity, and random integration of vector DNA. Moreover, recent studies have shown that proteins fused with a PTD composed of 11 poly-arginines (11R) effectively penetrates across the plasma membranes of various cells and show equivalent effects as that of adenovirus-mediated gene therapy.[19–21]

Received November 15, 2006; accepted November 21, 2006.

From Departments of Neurological Surgery (T.O., S.O., T.I., S.A., K.O., K.T., K.S., I.D.) and Physiology (K.T., H.M.), Okayama University Graduate School of Medicine, Dentistry, and Pharmaceutical Sciences, Shikata-cho, Okayama, Japan.

Correspondence to Tomoyuki Ogawa, Okayama University Graduate School of Medicine, Dentistry and Pharmaceutical Sciences, 2-5-1, Shikata-cho, Okayama 700-8558, Japan. E-mail tom@md.okayama-u.ac.jp

Stroke **is available at http://www.strokeaha.org** **DOI: 10.1161/01.STR.0000259887.70358.e0**

In this study, we examined the transduction efficiency of an 11R-fused enhanced green fluorescence protein (11R-EGFP; 27 kDa) into the vascular walls of model rats by intracisternal application of the fusion protein, compared with that of EGFP alone.

Materials and Methods

Experimental Groups

All animal studies were approved by the Animal Research and Care Committee at Okayama University Graduate School of Medicine, Dentistry, and Pharmaceutical Sciences.

Male Sprague-Dawley rats weighing 350 to 450 grams (Charles River Laboratories, Japan) were assigned to the following experiments.

Ex Vivo Protein Transduction

To examine time-dependent changes of the uptake of 11R-EGFP in the cerebral arteries, the rat BAs were treated with 11R-EGFP (12.5 μmol/L) in minimum essential medium (containing 0.1% bovine serum albumin, 100 U/mL penicillin, and 100 μg/mL streptomycin) at 37°C for 0 minutes, 10 minutes, 30 minutes, 2 hours, 6 hours, and 12 hours (n=5, each). The dose-dependency of the transduction of 11R-EGFP was next investigated. We varied the 11R-EGFP concentration. The rat BAs were harvested with each indicated concentration of 11R-EGFP (0.125 μmol/L, 1.25 μmol/L, and 12.5 μmol/L) for 2 hours (n=5, each). As a control, the rat BAs were also incubated with EGFP lacking 11R (12.5 μmol/L) (n=5) or phosphate-buffered saline (n=5) in the minimum essential medium. After treatment, the BAs were then cut into serial sections (16 μm) and observed under a fluorescent microscope (BX50, BX-FLA; Olympus).

In Vivo Protein Transduction Without SAH

Rats were anesthetized intraperitoneally with pentobarbiturate (70 mg/kg). A needle was inserted into the cisterna magna, and 250 μL of cerebrospinal fluid was withdrawn. The same volume of 11R-EGFP (12.5 μmol/L; n=5), EGFP (12.5 μmol/L; n=5), or saline (n=5) was infused. The rats were then euthanized with pentobarbiturate (700 mg/kg) in 2 or 6 hours, and the animals were fixed by perfusion with 100 mL of saline at physiological blood pressure. Finally, frozen sections of BA were cut 16-μm-thick and observed under the fluorescent microscope.

Western Blot Analysis of 11R-EGFP Expression

Cerebellums, brainstems, and BAs from the rats were dissected, and lysed by boiling and sonication containing 1% SDS. Samples were electrophoresed on 10% SDS-PAGE gels and then transferred to nitrocellulose membranes (Hybond ECL; Amersham Biosciences). The blots were probed with primary antibodies against polyclonal rabbit anti-GFP (1:200; sc-8334; Santa Cruz) and peroxidase-coupled secondary antibodies (1:2000; anti-rabbit IgG [H+L]; Pierce) before bands were visualized using a commercial ECL detection kit (Amersham Biosciences).

Immunohistochemistry

The BA sections were washed 3 times for 5 minutes each in 0.1 mol/L phosphate-buffered saline and then immersed for 5 minutes in 1.5% normal horse serum. The BA sections were then incubated with mouse monoclonal anti-rabbit smooth muscle cell antibodies (1:100; Abcam Ltd.) at 37°C for 30 minutes. Excess antibodies were washed off according to the manufacturer's recommendations, and then the sections were incubated with goat anti-rabbit IgG (H+L) rhodamine-conjugated secondary antibodies (1:200; CHEMICON International, Inc) for detection purposes.

Experimental Model of SAH

Rats were anesthetized by injection of pentobarbiturate (70 mg/kg). A 27-gauge catheter was then placed in the right radial artery, and autologous arterial blood was withdrawn. The atlanto-occipital membrane was exposed through a midline occipital incision and punctured with a 27-gauge needle into the cisterna magna; 200 μL of cerebrospinal fluid was withdrawn, after which 200 μL of autologous blood was slowly injected over a 5-minute period.

In Vivo Protein Transduction With SAH

The 11R-EGFP (250 μL, 15 μmol/L) or EGFP (250 μL, 15 μmol/L) was injected slowly (over 5 minutes) into the cisterna magna in rats immediately after the autologous blood injection (n=5, each). The rats were then euthanized using overdoses of anesthetic agents (pentobarbiturate) in 2, 6, 8, or 12 hours, and the animals were fixed by perfusion with 100 mL of saline. Finally, frozen sections of the BA were cut into 16-μm-thick and observed under a fluorescent microscope.

Fluorescence Measurement

We examined the fluorescence intensity of 11R-EGFP or EGFP itself. The analysis was performed using Scion imaging software (Scion Corporation).

Statistical Analysis

Data are shown as the mean (±standard deviation). Data were analyzed using 1-way or 2-way ANOVA followed by planned comparisons of multiple conditions. $P<0.05$ was considered to be significant.

Results

Transduction of 11R-EGFP Into the Cerebral Arteries Ex Vivo

Green fluorescence of 11R-EGFP was faint at 10 minutes but increased over time, achieving a steady-state level in 2 hours. The high expression persisted longer than 12 hours (Figure 1A and 1C). In the BAs incubated with each indicated concentration of 11R-EGFP, the intense green fluorescent signals increased depending on 11R-EGFP concentration (Figure 1B and 1D). EGFP lacking 11R was not observed in the BAs, whereas 11R-EGFP strongly transduced into all layers of the rat BAs.

Transduction of 11R-EGFP Into the Cerebral Arteries In Vivo

The 11R-EGFP was transduced into the arterial wall (2 or 6 hours after injection) in the in vivo model (Figure 2A and 2C). EGFP lacking 11R was not delivered into the arterial wall, although green signals indicating aggregation of EGFP in the subarachnoid space were observed (Figure 2B and 2D). To investigate the transduction efficacy of the proteins in BAs of normal rats, we examined the fluorescence intensity of arterial walls 2 hours after injection. The 11R-EGFP exhibited a diffuse, highly fluorescent signal in all layers, especially in the tunica media, of the cerebral arteries compared with EGFP lacking 11R (Figure 3A). Interestingly, 11R-EGFP fluorescence was colocalized with the smooth muscle layer (Figure 3B, a through c). Western blot analysis reproducibly revealed a robust EGFP transduction in 11R-EGFP–treated animals. No protein transduction was detectable in control animals. Interestingly, 11R-EGFP was selectively introduced into the BAs (Figure 3C).

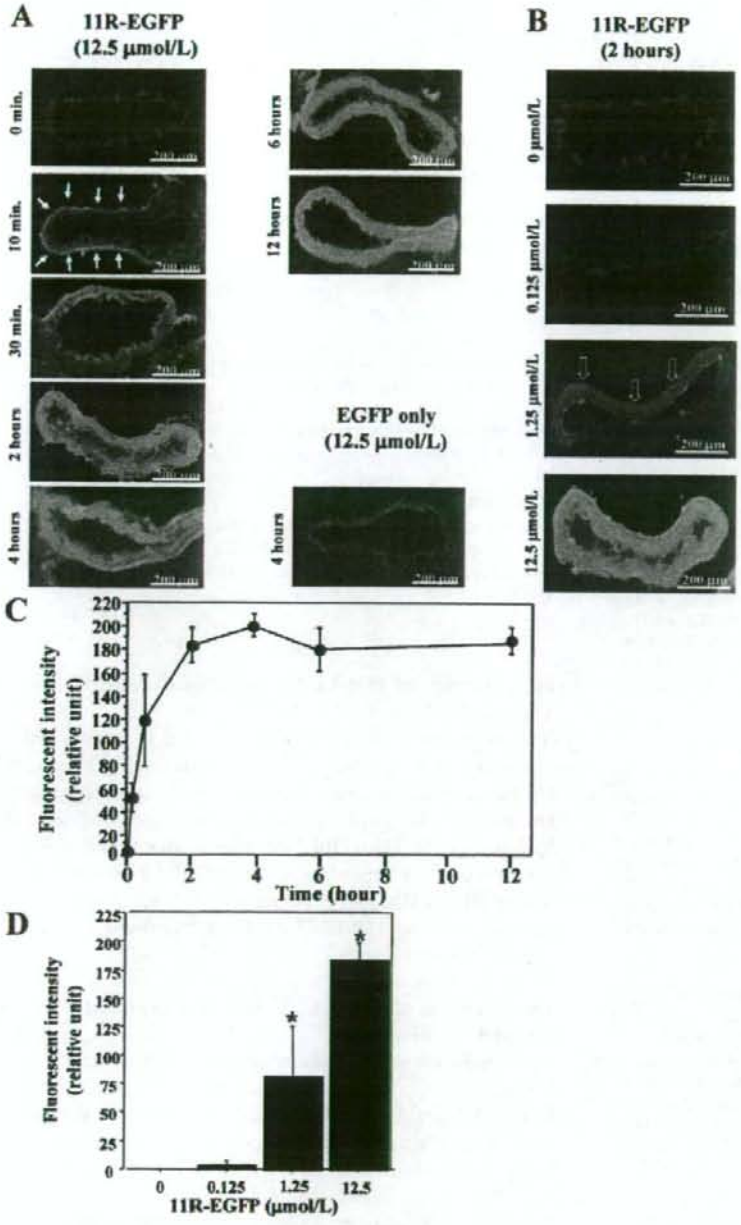

Figure 1. A, Time-dependent changes of the level of transduced 11R-EGFP in BAs ex vivo. At the time indicated after the addition of 12.5 μmol/L of 11R-EGFP, the BAs were washed once with phosphate-buffered saline and observed under the fluorescent microscope. The 11R-EGFP existed mainly in the adventitia overlying BAs in 10 minutes (solid arrows). However, 11R-EGFP was strongly transduced into all layers of the BAs in 2 hours. B, Dose-dependent transduction of 11R-EGFP into rat BAs. Two hours after adding 11R-EGFP at the indicated concentrations, the BAs were washed once with phosphate-buffered saline and observed under the fluorescent microscope. The fluorescence was seen at the contact surface exposed to 1.25 μmol/L of 11R-EGFP (open arrows), while the high level of the expression was observed in all layers of BAs after the injection of 12.5 μmol/L of 11R-EGFP. C and D, Quantification of the incorporated 11R-EGFP protein in the rat BAs. The fluorescent intensity (arbitrary unit) of each BA in A (left) and B (right) were estimated by using the Scion Image program to obtain averages with standard deviation (vertical bars). Exposure time was identical within each experiment. *$P<0.0001$ according to ANOVA.

11R-Mediated EGFP Transduction Into the Cerebral Arteries After SAH Induction

Light and direct fluorescence microscopies were used to assess the extent of transduction of the proteins into the BAs of SAH rats. Light microscopic analysis of sections stained with hematoxylin-eosin revealed the presence of typical subarachnoid clots (Figure 4B and 4D). The sections of the rat BAs in the SAH group treated with 11R-EGFP showed a fluorescence pattern distributed throughout the arterial wall, even though there was a lot of clotted blood in the subarachnoid space (Figure 4A and 4B). However, Figure 4C shows a distinct lack of tissue fluorescence (except for the autofluorescence in the internal elastic lamella) in arterial tissue treated with EGFP lacking 11R.

To examine the distribution of 11R-EGFP in the subarachnoid space, we compared the fluorescent image with the hematoxylin-eosin staining image at 2 hours after injection. The 11R-EGFP showed a strong fluorescent signal in the arterial wall, but was not observed in the brain parenchyma (Figure 5A and 5B). To investigate the transduction efficacy of the proteins in the BAs exposed to SAH, we examined the fluorescence intensity of the arterial walls at 2 hours after

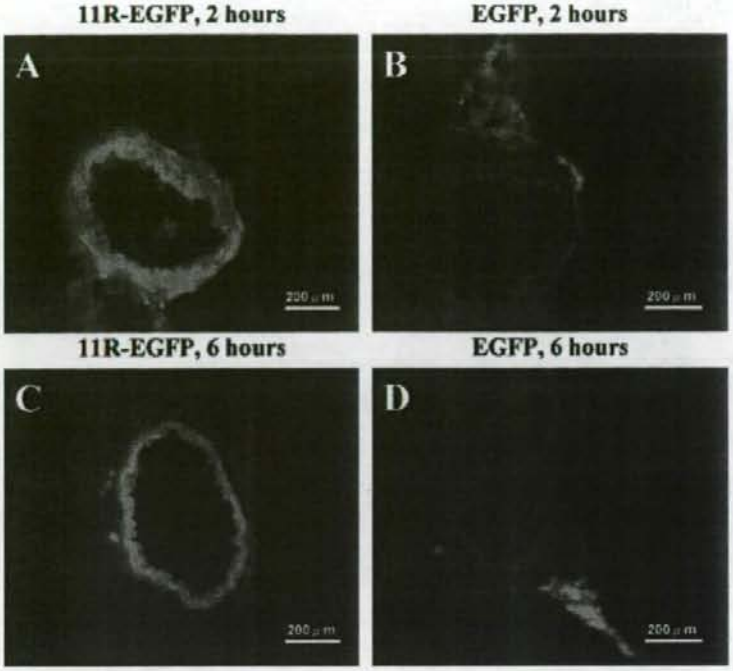

Figure 2. Protein transduction of 11R-EGFP in BAs, in vivo (without SAH). The 11R-EGFP (12.5 μmol/L) (A, C) or EGFP (12.5 μmol/L) (B and D) was injected into the cisterna magna. BAs and brain stems were dissected from rats 2 hours (A and B) or 6 hours (C and D) after the injection, sectioned (in 16-μm sections), and observed by fluorescent microscopy. The 11R-EGFP was transduced into the arterial wall 2 or 6 hours after the injection (A and C). EGFP lacking 11R was not observed in the arterial wall, although it was found in the subarachnoid space (B and D).

injection. The fluorescence of the BA was more intense in the SAH rats injected with 11R-EGFP than those injected with EGFP lacking 11R or saline. Interestingly, this finding was especially prominent in the tunica media, a finding that was also encountered in the case of the normal (no SAH) rats (Figure 5C).

Time-Dependent Changes of 11R-EGFP Expression in the BAs After SAH Induction

A high level of 11R-EGFP was detected in the rat BAs within 2 hours after the addition of the protein. However, the protein gradually degraded over a 12-hour period (Figure 6).

Discussion

Previous studies showed that the PTD of the HIV type 1 transcriptional activator of transcription (TAT) protein, which contains a high proportion of arginine and lysine residues, has been identified as being responsible for the ability to penetrate the plasma membrane.[17,22,23] This PTD was shown to serve as a carrier for directing the uptake of heterologous proteins into cells by generating genetic in-frame PTD fusion proteins.[24–26] Interestingly, the PTD of the TAT protein can deliver the biologically active form of β-galactosidase (120 kDa), which consists of >1000 amino acids, to all tissues, including the brain, in vivo.[22] Recent studies have shown that 11-residue poly-arginine peptides (11R) have higher transduction activity than the PTD of the TAT protein and are useful for protein delivery in cells.[27–29] For these reasons, we used 11R as the PTD in the present study.

The mechanisms of protein transduction of PTD-fusion proteins into cells were investigated by many previous studies. Early mechanistic studies showed that TAT-mediated transduction occurs through a rapid temperature- and energy-independent process, suggesting direct penetration across the lipid bilayer.[17,18] Wadia et al[29] showed that TAT fusion proteins were rapidly internalized by lipid raft-dependent macropinocytosis, and most of the internalized proteins were entrapped in macropinosomes. A recent study showed that 11R PTD fused with the influenza virus hemagglutinin-2 protein, which has the beneficial aspect of disrupting only macropinosomes but no other types of vesicles, markedly enhanced the effect of fusion proteins. The authors showed that the linking of hemagglutinin-2 protein with 11R-p53 protein induced delivery into nucleus of glioma cells and strongly enhanced the anticancer effect of p53, providing that 11R fusion proteins function by the same mechanism of internalization into cells as TAT fusion proteins.[30]

Previous reports showed that HIV–TAT-fused proteins were delivered into various tissues, including brain parenchyma through the blood–brain barrier several hours after intravenous or intraperitoneal injection.[22,31–33] In our experiments, 11R-EGFP was effectively introduced into vascular walls a few hours after intracisternal injection both in vivo and ex vivo (Figures 1 and 2). This result may indicate that 11R-fusion proteins have an immediate effect on cerebral arteries. Moreover, by intrathecal administration, 11R-EGFP was not translocated into the brain parenchyma, but selectively into the rat BAs (Figures 3C and 5). Therefore, this 11R-based transcisternal protein transduction method may be an immediately effective and highly selective treatment for cerebral arteries.

Previous reports suggested that the efficiency of virus-mediated gene delivery was limited because transgene expression was observed only in adventitia of blood vessels but

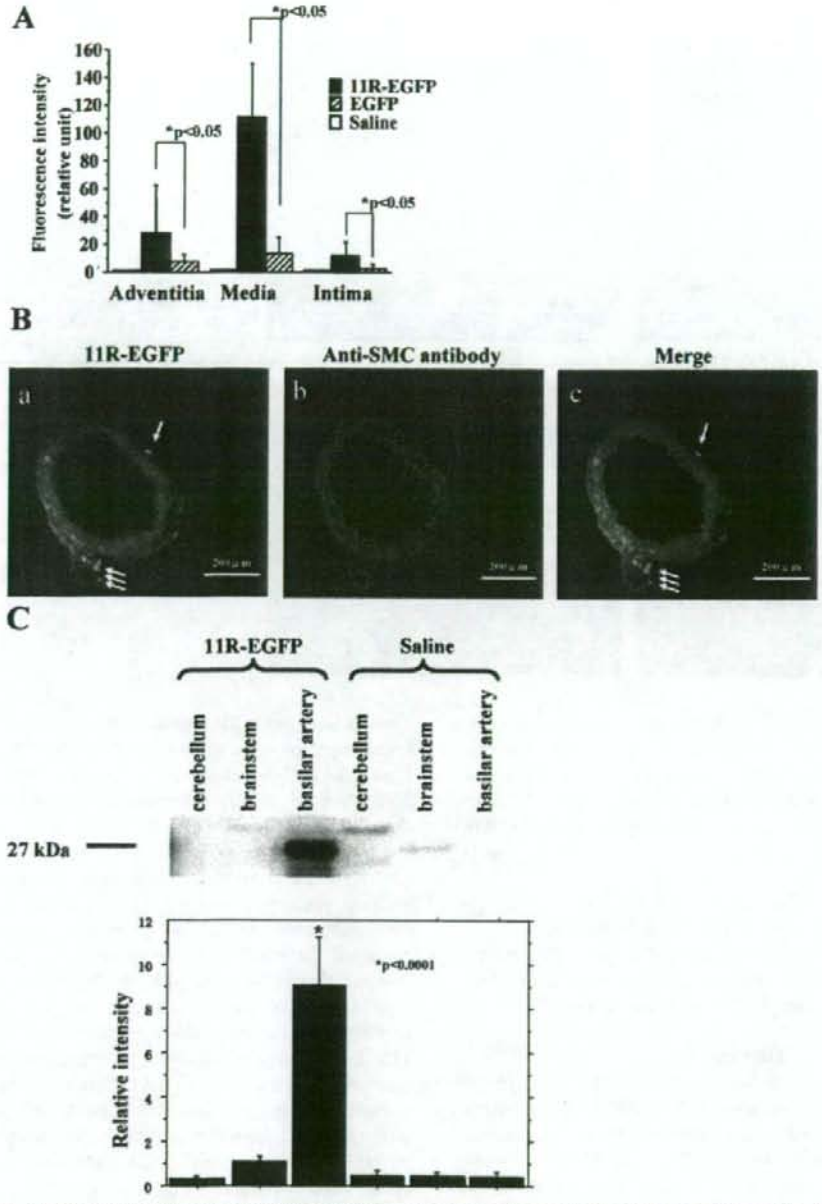

Figure 3. Intensity of fluorescence detected in basilar artery segments of normal rats 2 hours after the injection (A). The 11R-EGFP was transduced mainly into the tunica media of normal basilar arteries. The fluorescence was much more intense in BAs from rats injected with 11R-EGFP than those from intact rats or rats injected with EGFP. Interestingly, this tendency was especially prominent in the tunica media. Signals were analyzed by Scion Image (n=15 slices, each). Localization of 11R-EGFP in the BA (B). 11R-EGFP localization (green; a) and immunohistochemical analysis (b) of the smooth muscle cell layer in the BA. Merged image (c) with 11R-EGFP (green) and the smooth muscle cell layer (red). The merged image showed that the high level of expression of 11R-EGFP was colocalized with the smooth muscle layer in a normal rat. Arrows indicate the protein bodies of 11R-EGFP themselves around the blood vessels. They are about to enter into the walls of the BAs. C, Western blot analysis of EGFP transduction in saline and 11R-EGFP–treated animals 2 hours after intracisternal infusion of protein. Note the high level of 27 kDa EGFP in the 11R-EGFP–treated vs saline-treated animal. Bar graph (bottom) showing semiquantification of EGFP bands for each group (n=3, each). *$P<0.0001$ according to ANOVA.

not in either vascular muscle or endothelium.[7,34,35] In the present study, we found that intracisternal protein transduction using an 11R-fusion protein selectively delivered this protein into cerebral vessels, and the delivered protein was especially transduced into the tunica media (smooth muscle layer) of the BA (Figure 3), even when it had been exposed to SAH (Figures 4, 5). This finding suggests that this protein transduction method may be a more effective therapeutic

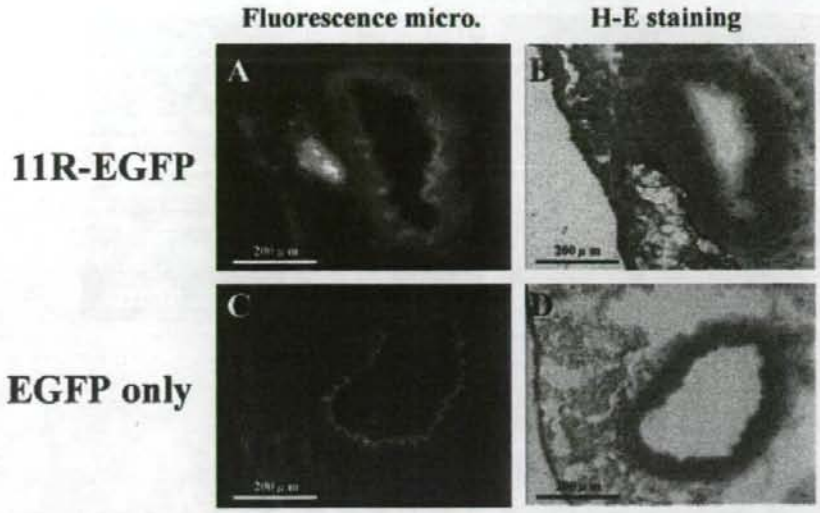

Figure 4. Protein transduction of 11R-EGFP in BAs, in vivo (with SAH). Rats were given an injection of 11R-EGFP (A and B) or EGFP (C and D) into the cisterna magna immediately after 0.25 mL of autologous arterial blood was injected. BAs and brain stems were dissected from rats, sectioned (in 16-μm sections), and observed by light and direct fluorescence microscopy. Fluorescent microscopic images (A and C) and hematoxylin-eosin staining (B and D). (A) is the same section as (B), and (C) is the same section as (D).

method for treatment of cerebral arteries than viral vector-mediated gene transduction therapy.

The high expression of 11R-EGFP was maintained when the BAs were kept on incubating with 11R-EGFP for 12 hours ex vivo (Figure 1). At the same time, the elevated expression level of 11R-EGFP was gradually decreased during 12 hours in blood vessels with only a single injection of 11R-EGFP in vivo (Figure 6). These results indicated that repeated administration of 11R-fused proteins might be needed to maintain a desired therapeutic effect. It has also been claimed that protein therapy is superior to viral vector-mediated gene therapy in terms of inflammatory response.[7] Previous studies indicated that PTD-fused p53 was not toxic and did not affect normal cells, whereas adenovirus-p53 significantly induced detrimental effects in normal cells.[19,30] We also found that there was no immunoreactivity after injection with 11R-EGFP in this study. Moreover, Schwarze et al[22] examined the potential immune responses and toxicity associated with long-term transduction of PTD fusion proteins and noted that injection of a mouse with 1 mg of a TAT PTD fusion protein per kilogram of body weight each day for 14 consecutive days produced no signs of gross neurological problems or systemic distress. However, for blood vessels, these matters with long-term transduction of the proteins have not been elucidated in detail yet. Therefore, a protein therapy that will reliably transduce stable proteins into blood vessels needs to be developed. Before initiating clinical trials of protein transduction therapy for treatment of cerebral arteries, the remaining challenges of protein therapy noted must be overcome.

Future Perspectives

The present report shows that 11R-EGFP was transduced effectively into all layers of rat cerebral arteries at least 2 hours after the injection of the protein. However, the expression in cerebral arteries was not maintained for a long time

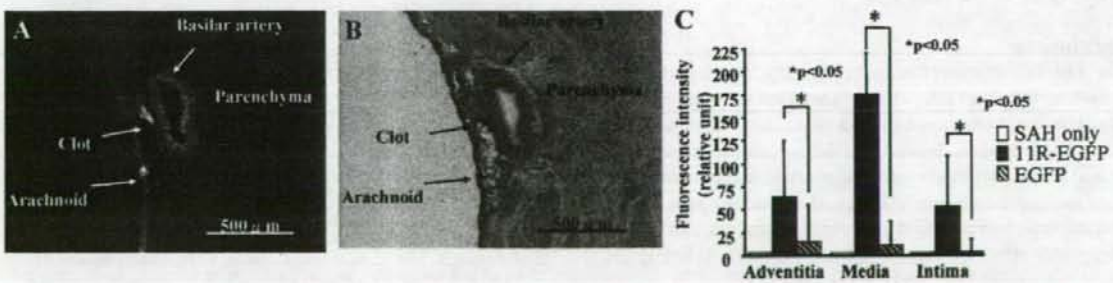

Figure 5. Distribution of 11R-EGFP in the subarachnoid space 2 hours after injection (A and B). The 11R-EGFP existed mainly within the vascular wall, but was not observed in the brain parenchyma. Fluorescent microscopic image (A) hematoxylin-eosin staining (B). Intensity of fluorescence detected in basilar artery segments of SAH rats 2 hours after injection (C). As in the case of normal rats, the fluorescence was much more intense in the arterial walls, especially in the tunica media of SAH rats injected with 11R-EGFP than those injected with EGFP. Signals were analyzed by Scion Image.